



FEDERAL UNIVERSITY OF AMAZONAS



GRADUATE PROGRAM IN MATERIALS SCIENCE AND ENGINEERING

**Chemically synthesized poly(*o*-methoxyaniline): Influence of counterions  
on the structural and electrical properties**

MATHEUS MORAES BIONDO

Manaus/AM  
November, 2019

MATHEUS MORAES BIONDO

**Chemically synthesized poly(*o*-methoxyaniline): Influence of counterions  
on the structural and electrical properties**

Dissertation submitted in fulfillment of the  
requirements for the Degree of Master in  
Materials Science and Engineering.

**Advisor:** Prof. Dr. Edgar Aparecido Sanches

Manaus/AM  
November, 2019

### Ficha Catalográfica

Ficha catalográfica elaborada automaticamente de acordo com os dados fornecidos pelo(a) autor(a).

B615c Biondo, Matheus Moraes  
Chemically synthesized poly(o-methoxyaniline): Influence of counterions on the structural and electrical properties / Matheus Moraes Biondo. 2019  
56 f.: il. color, 31 cm.

Orientador: Dr. Edgar Aparecido Sanches  
Dissertação (Mestrado em Ciência e Engenharia de Materiais) -  
Universidade Federal do Amazonas.

1. Poly(o-methoxyaniline). 2. Le Bail method. 3. electrical conductivity. 4. charge carriers. I. Sanches, Dr. Edgar Aparecido II. Universidade Federal do Amazonas III. Título

**PARECER DE BANCA EXAMINADORA DE QUALIFICAÇÃO**

Nós, da Banca Examinadora de Defesa de Dissertação de Mestrado do:

Aluno: **MATHEUS MORAES BIONDO**  
Curso: **Ciência e Engenharia de Materiais**  
Orientador (a): **Prof. Dr. Edgar A. Sanches**  
Título do Projeto: **“Chemically synthesized poly(*o*-methoxyaniline): Influence of counterions on the structural and electrical properties”**

Em sessão pública realizada no dia 22 de novembro de 2019 na Sala José Leitão do Bloco de Estatística do Instituto de Ciências Exatas - ICE, no Setor Norte do Campus Universitário da Universidade Federal do Amazonas - UFAM, consideramos o candidato:

APROVADO

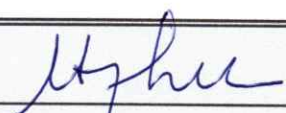
NÃO APROVADO

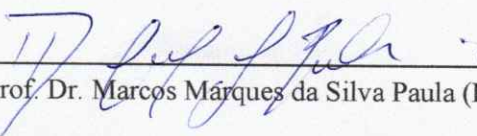
Considerações:

\_\_\_\_\_

\_\_\_\_\_

\_\_\_\_\_

  
\_\_\_\_\_  
Prof. Dr. Edgar A. Sanches (PPGCEM)

  
\_\_\_\_\_  
Prof. Dr. Marcos Márques da Silva Paula (PPGCEM)

  
\_\_\_\_\_  
Dra. Lianet Aguilera Dominguez (UFAM)

Ciente do Aluno:

  
**MATHEUS MORAES BIONDO**

Manaus (AM), 22 de novembro de 2019.

## ACKNOWLEDGMENTS

- ❖ To **God** for allowing the development of this work and also for all the achievements that have brought me here.
- ❖ To my parents **Maria José Paz Moraes** and **Alberto Antônio Biondo** for their unconditional love and for guiding me to the path of study.
- ❖ To my brother **Lucas Moraes Biondo**, my best friend, for supporting me all the time.
- ❖ To my advisor **Prof. Dr. Edgar Aparecido Sanches**, for his commitment and dedication, as well as his valuable teachings that I will always take with me.
- ❖ To my dear friends and coworkers from NANOPOL who provided a motivating, collaborative, and laughing work environment: **Adriano de Souza Carolino, Ana Luisa Farias Rocha, André Andrade Ferreira, Ayná Caroline Marcião Vieira, Bianca de Andrade Feitosa, Ítalo Ricardo Serrão Bezerra, Jéssica Montenegro Santana da Silva, Joab de Souza Arouche, Josiana Moreira Mar, Laiane Souza da Silva, Larissa Medeiros de Oliveira, Lilian Rodrigues de Oliveira, Márcia Cristina Gomes de Araújo Lima, Matheus Fonseca Ferreira, Maxwaldo da Silva Rabelo, Paulo Victor Rodrigues Gomes, Sidney Gomes Azevedo, Suzan Xavier Lima, Tiago Neves Veras, Yngra Karolyne Jaques Wadick** and **Yuri Gomes**.
- ❖ To the dear friendships formed during this journey: **Aércio Filipe Franklim de Figueiredo Pereira, Alexandra Lizandra Gomes Rosas, Augusto Dias Melo, Bruna Bandeira do Nascimento, Camila da Costa Pinto, Cíndel Cavalcante de Souza, Ítalo Carvalho da Costa, Profa. Dra. Jaqueline de Araújo Bezerra, Jorge de Souza Passos Junior, Juliana Pereira da Silva, Leonardo Arcanjo, Miécio de Oliveira Melquiades, Prof. Dr. Pedro Henrique Campelo Felix, Philipi Cavalcante Ricardo, Ricardo Ito de Messias** and **Sabrina da Silva Santana**.
- ❖ To Prof. Dr. Sérgio Michielon de Sousa and Prof. Dr. Yurimiler Leyet Ruiz for their scientific contribution.
- ❖ To Laboratory of Nanostructured Polymers – NANOPOL, for the infrastructure and welcoming working environment.
- ❖ To **LabMat (UFAM), LPMat (UFAM)** and **LMEA (IFSC-USP)** for the performed analyzes of X-ray Diffraction, Complex Impedance Spectroscopy and Scanning Electron Microscopy.
- ❖ To the Graduate Program in Materials Science and Engineering (PPGCEM-UFAM) for providing this opportunity.

## ABSTRACT

Poly(*o*-methoxyanilines) (POMA) were chemically synthesized using different dopant acids to obtain the polymers POMA/HCl, POMA/HNO<sub>3</sub>, POMA/H<sub>2</sub>SO<sub>4</sub> and POMA/H<sub>3</sub>PO<sub>4</sub>. The nature and size of the counterions influenced considerably on the structural, morphological, thermal and electrical properties of the as-synthesized polymers. X-ray Diffraction (XRD) patterns presented slightly peak displacements according to the dopant acid, influencing the lattice parameters specially along [010]. The polymers POMA/HCl, POMA/HNO<sub>3</sub> and POMA/H<sub>2</sub>SO<sub>4</sub> presented similar percentage of crystallinity (around 50 %), while the polymer POMA/H<sub>3</sub>PO<sub>4</sub> was the less crystalline (around 40 %). Polymer morphology was dependent on the dopant acid, besides multimorphologies were observed in the polymers POMA/HCl, POMA/HNO<sub>3</sub> and POMA/H<sub>3</sub>PO<sub>4</sub>. A great counterion influence from the doping acid was found in the electrical properties. The total variation obtained in DC conductivity was five orders of magnitude. The calculated values were  $6.6 \times 10^{-1}$  S/cm,  $1.11 \times 10^{-2}$  S/cm,  $3.64 \times 10^{-3}$  S/cm and  $5.2 \times 10^{-4}$  S/cm for POMA/HCl, POMA/HNO<sub>3</sub>, POMA/H<sub>2</sub>SO<sub>4</sub> and POMA/H<sub>3</sub>PO<sub>4</sub>, respectively. The use of HCl as dopant potentiated the DC conductivity of the polymeric material.

**Keywords:** Poly(*o*-methoxyaniline), Le Bail method, electrical conductivity, charge carriers.

## RESUMO

Poli(*o*-metoxianilinas) (POMA) foram sintetizadas quimicamente usando diferentes ácidos dopantes para obter os polímeros POMA/HCl, POMA/HNO<sub>3</sub>, POMA/H<sub>2</sub>SO<sub>4</sub> e POMA/H<sub>3</sub>PO<sub>4</sub>. A natureza e o tamanho dos contra-íons influenciaram consideravelmente nas propriedades estruturais, morfológicas, térmicas e elétricas dos polímeros sintetizados. Os padrões de difração de raios X (DRX) apresentaram deslocamentos de pico de acordo com o ácido dopante, influenciando nos parâmetros da rede especialmente ao longo da direção [010]. Os polímeros POMA/HCl, POMA/HNO<sub>3</sub> e POMA/H<sub>2</sub>SO<sub>4</sub> apresentaram percentuais semelhantes de cristalinidade (em torno de 50 %), enquanto o polímero POMA/H<sub>3</sub>PO<sub>4</sub> foi o menos cristalino (em torno de 40 %). A morfologia polimérica foi dependente do ácido dopante, e multimorfologias foram observadas nos polímeros POMA/HCl, POMA/HNO<sub>3</sub>, POMA/H<sub>2</sub>SO<sub>4</sub> e POMA/H<sub>3</sub>PO<sub>4</sub>. Considerável influência do contra-íon proveniente do ácido dopante foi constatada nas propriedades elétricas. A variação total obtida na condutividade DC foi de cinco ordens de magnitude. Os valores calculados foram  $6,6 \times 10^{-1}$  S/cm,  $1,11 \times 10^{-2}$  S/cm,  $3,64 \times 10^{-3}$  S/cm e  $5,2 \times 10^{-4}$  S/cm para POMA/HCl, POMA/HNO<sub>3</sub>, POMA/H<sub>2</sub>SO<sub>4</sub> e POMA/H<sub>3</sub>PO<sub>4</sub>, respectivamente. O uso de HCl como dopante potencializou a condutividade elétrica do material polimérico.

**Palavras-chave:** Poli(*o*-metoxianilina), método de Le Bail, condutividade elétrica, portadores de carga.



## LIST OF FIGURES

<b>Figure 1</b> - Schematic representation of a conjugated chain containing alternating single and double bonds.....	2
<b>Figure 2</b> - (a) $\sigma$ bond formation from the overlap of the $sp^2$ orbitals; (b) formation of the $\pi$ bond in a plane perpendicular to the plane of the main chain and (c) delocalization of the $\pi$ -conjugated system above and below the main polymer chain.....	3
<b>Figure 3</b> -(a) Conventional representation of the electronic band energy structure for a solid material at equilibrium interatomic spacing. (b) Electron energy versus interatomic separation for a cluster of atoms .....	4
<b>Figure 4</b> - Energy diagram of a semiconductor material.....	5
<b>Figure 5</b> - HOMO and LUMO bands of conjugated organic molecules.....	6
<b>Figure 6</b> - Polaron electron and polaron hole band structure.....	7
<b>Figure 7</b> - Conduction mechanism of doped polymers (a) indicating intrachain charge transport, (b) indicating interchain transport, (c) indicating interparticle transport. Arrows showing the path of the charge carrier migrating through the material. ....	8
<b>Figure 8</b> - Map of forces obtained by Atomic Force Microscopy (AFM) showing conducting islands of poly( <i>o</i> -ethoxyaniline) film. ....	9
<b>Figure 9</b> - Generalized representation of the most common forms of PANI.....	10
<b>Figure 10</b> - Molecular structure of a POMA tetramer as (a) Emeraldine-base (POMA-EB) and (b) Emeraldine-salt (POMA-ES) forms. ....	12
<b>Figure 11</b> - Electrical conductivity (S/cm) of materials .....	13
<b>Figure 12</b> - (a) X-ray diffraction patterns of the polymers POMA/HCl, POMA/HNO <sub>3</sub> , POMA/H <sub>2</sub> SO <sub>4</sub> and POMA/H <sub>3</sub> PO <sub>4</sub> and (b) the angular region $2\theta = 5 - 30^\circ$ highlighting the most intense diffraction peaks.....	18
<b>Figure 13</b> - Peak deconvolution of the polymers (a)POMA/HCl, (b)POMA/HNO <sub>3</sub> , (c)POMA/H <sub>2</sub> SO <sub>4</sub> and (d)POMA/H <sub>3</sub> PO <sub>4</sub> . XRD patterns (black curves) were fitted (red curves) by using the Gaussian function (green curves). The blue curves are due to the non-crystalline contribution.....	20
<b>Figure 14</b> - Crystallite shape projections for the polymers (a) POMA/HCl, (b) POMA/HNO <sub>3</sub> , (c) POMA/H <sub>2</sub> SO <sub>4</sub> and (d) POMA/H <sub>3</sub> PO <sub>4</sub> along [100], [010] and [001].....	23
<b>Figure 15</b> - FTIR spectra of the polymers POMA/HCl, POMA/HNO <sub>3</sub> , POMA/H <sub>2</sub> SO <sub>4</sub> and POMA/H <sub>3</sub> PO <sub>4</sub> . ....	25
<b>Figure 16</b> - SEM images of the as-synthesized POMA/HCl. ....	26



<b>Figure 17</b> - SEM images of the as-synthesized POMA/HNO <sub>3</sub> .....	27
<b>Figure 18</b> - SEM images of the as-synthesized POMA/H <sub>2</sub> SO <sub>4</sub> .....	28
<b>Figure 19</b> - SEM images of the as-synthesized POMA/H <sub>3</sub> PO <sub>4</sub> .....	29
<b>Figure 20</b> - TG/dTG curves of the polymers POMA/HCl, POMA/HNO <sub>3</sub> , POMA/H <sub>2</sub> SO <sub>4</sub> and POMA/H <sub>3</sub> PO <sub>4</sub> . .....	30
<b>Figure 21</b> - AC electrical conductivity as a function of the frequency for the polymers POMA/HCl, POMA/HNO <sub>3</sub> , POMA/H <sub>2</sub> SO <sub>4</sub> and POMA/H <sub>3</sub> PO <sub>4</sub> .....	32

## LIST OF TABLES

<b>Table 1</b> - Diffraction peak positions ( $2\theta$ ) of POMA/HCl, POMA/HNO <sub>3</sub> , POMA/H <sub>2</sub> SO <sub>4</sub> and POMA/H <sub>3</sub> PO <sub>4</sub> . .....	21
<b>Table 2</b> - Le Bail method performed for the polymers POMA/HCl, POMA/HNO <sub>3</sub> , POMA/H <sub>2</sub> SO <sub>4</sub> and POMA/H <sub>3</sub> PO <sub>4</sub> using the program Fullprof: lattice parameters, unit cell volume, crystallite average size, and agreement factors ( $R_{wp}$ , $R_p$ and $\chi^2$ ). .....	22
<b>Table 3</b> - TGA/dTG events of the polymers POMA/HCl, POMA/HNO <sub>3</sub> , PMA/H <sub>2</sub> SO <sub>4</sub> and POMA/H <sub>3</sub> PO <sub>4</sub> . .....	30

## TABLE OF CONTENTS

1. INTRODUCTION .....	1
2 LITERATURE REVIEW .....	2
2.1 Conjugated Polymers .....	2
2.2 Electrical Conduction Mechanism .....	3
2.3 Charge Transport.....	8
2.4 Polyaniline.....	9
2.5 Poly( <i>o</i> -methoxyaniline).....	11
2.6 Influence of Dopant Acids on the Properties of Conjugated Polymers .....	13
2.7 Applications of Conjugated Polymers .....	14
3 EXPERIMENTAL .....	16
3.1 Polymer Synthesis .....	16
3.2 XRD Analysis and Percentage of Crystallinity .....	16
3.3 Le Bail Method .....	16
3.4 SEM Analysis.....	17
3.5 Fourier-transform Infrared Spectroscopy (FTIR) Analysis .....	17
3.6 Thermogravimetric Analysis (TG/dTG) .....	17
3.7 Complex Impedance Spectroscopy analysis (CIS) .....	17
4 RESULTS AND DISCUSSIONS.....	18
4.1 X-ray Diffraction Analysis and Percentage of Crystallinity .....	18
4.2 Le Bail Method .....	21
4.3 FTIR Analysis .....	24
4.4 SEM Analysis.....	26
4.5 TG/dTG Analysis .....	29
4.6 Complex Impedance Spectroscopy Analysis .....	31
CONCLUSIONS.....	35
ACKNOWLEDGMENTS .....	35
REFERENCES.....	36

## 1. INTRODUCTION

Considerable efforts have been devoted to correlate synthesis conditions with structural and electrical properties of chemically synthesized conjugated polymers. The doping process is decidedly dependent on the nature of the dopant acid[1], and conformational modifications of these polymers are influenced by the substituents electron donating groups present along the aromatic rings[2]. For this reason, the functionalized side groups at the *ortho*, *meta* or *para* positions in polyaniline (PANI) derivatives, such as poly(*o*-methoxyaniline) - POMA, allowed a range of physicochemical properties[3]. Structural, morphological, thermal and electrical properties of *ortho*-substituted polyanilines have been widely discussed [4–6]. However, to the best of our knowledge, no systematic studies have been reported on the relationship between the influence of doping acids on the properties of POMA.

The conduction mechanism of conjugated polymers results in the generation and disappearance of charged sites, while electroneutrality is maintained by mobile counterions[7]. Moreover, the physicochemical properties of these macromolecules also depend on the counterion of the Brønsted doping acid. The protonation equilibrium involves exclusively the quinone diimine segment of the polymer chain, while the number of electrons remain constant. The charged centers can move along the conjugated system by the rearrangement of the double and single bonds in the presence of an electric field[7]. For this reason, the nature and size of counterions have significant influence on the electrical conductivity of conjugated polymers.

In order to evaluate the effect of different counterions on the structural, morphological, thermal and electrical properties of POMA, we prepared polymers using HCl, HNO<sub>3</sub>, H<sub>2</sub>SO<sub>4</sub> and H<sub>3</sub>PO<sub>4</sub> as dopant acids. X-ray diffraction technique (XRD) was carried out in order to examine the long-range order achieved as a consequence of very short-range interactions. The Le Bail method[8] was performed in the Fullprof program using the previous XRD patterns to refine cell parameters and assess crystallite size. Peak broadening based on linear combination of spherical harmonics was useful to evaluate the anisotropic crystallite shape. FTIR spectroscopy was performed aiming a molecular structural characterization. Scanning Electron Microscopy (SEM) was useful to correlate the nature of the counterions with the resulted polymer morphology. Thermal analysis (TG/dTG) were conducted to evaluate the polymer thermal stability as a function of different dopant acids. Then, these results were correlated with the electrical conductivity results obtained by Complex Impedance Spectroscopy analysis.

## 2 LITERATURE REVIEW

### 2.1 Conjugated Polymers

Polymeric materials had been classified for many years as insulating and dielectric materials because their strong and directional covalent bonds do not allow the necessary mobility of charge carriers. The idea that polymeric materials could present electrical conductivity seemed scientifically impossible until the 1970s until the discovery of the so-called *synthetic metals* or *conjugated polymers*[9]. These materials are *Intrinsically Conducting Polymers (ICP)*, which are formed by chains containing double conjugated C=C bonds, which allow an electron flow under specific conditions[9,10], as shown in **Figure 1**.

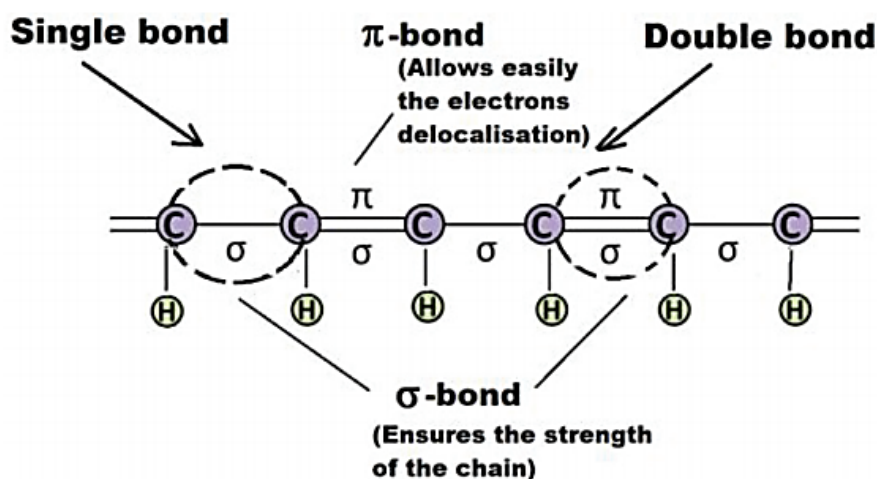


**Figure 1** - Schematic representation of a conjugated chain containing alternating single and double bonds.

The electronic structure of conjugated polymers can be described by the overlapping of the  $p_z$  orbitals originated from  $sp_2 + p_z$  hybridized carbon atoms. The carbon atoms of the main polymeric chain are bonded by the  $\sigma$  bonds, which are formed by the overlapping of the  $sp_2$  hybrid orbitals of each atom, as shown in **Figure 2(a)**. The interactions between the  $p_z$  orbitals are weaker than those observed in the  $sp_2$  orbitals of the  $\sigma$  bond. However, the  $\pi$  bonds are formed in a plane perpendicular to that of the main chain, resulting in the occupied  $\pi$ -ligand molecular orbitals, and in the  $\pi^*$ -antiligand orbitals, represented by  $\pi^*$ , as indicated in **Figure 2(b)**. These orbitals are delocalized above and below of the main polymeric backbone, as shown in **Figure 2(c)**.

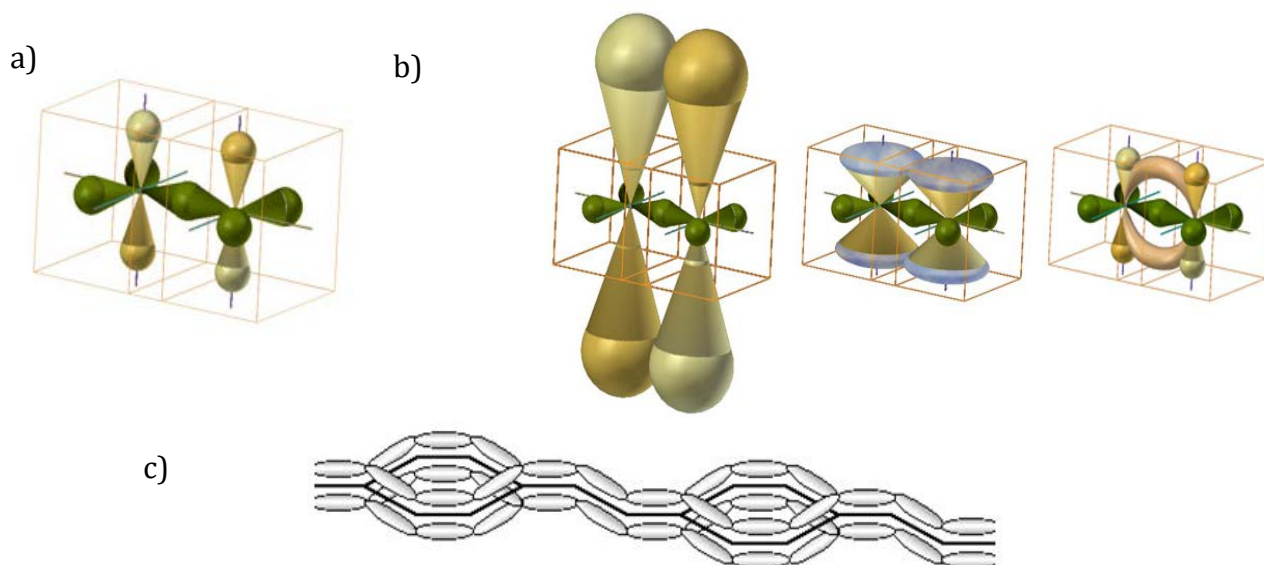


**Figure 2** - (a)  $\sigma$  bond formation from the overlap of the  $sp^2$  orbitals; (b) formation of the  $\pi$  bond in a plane perpendicular to the plane of the main chain and (c) delocalization of the  $\pi$ -conjugated system above and below the main polymer chain [13].

The delocalization of the  $\pi$ -conjugated system observed throughout the main polymer chain allows the mobility of charges along the polymeric structure and between adjacent chains under specific conditions. However, the conjugated structure is not sufficient for the electrical conductivity occurrence, and a doping process is needed. The insertion of electrons or formation of vacancies that move along the chain result in the electrical conduction phenomenon in the conjugated polymers[11]. However, some factors influence on the electrical conductivity and, therefore, on the mobility of the charge carriers, such as structural disorder, coulombian interactions between electrons and holes, as well as the size of the doping counterions[12].

## 2.2 Electrical Conduction Mechanism

The conductive properties of polymeric materials are basically restricted to those presenting a conjugated structure, from insulator to conductor, through reversible oxidation (or reduction) processes of the  $\pi$ -conjugated system[13–16]. Oxidation (or reduction) reactions in the polyenic polymer chain caused by acid dopants result in the formation of delocalized polymeric ions, which can be neutralized by the incorporation of anions (or cations)[14,17]. The doping process may be carried out by chemical methods or only by exposing the polymers to the vapors of charge transfer agents. In most conjugated polymers,

the doping process occurs simultaneously with the chain oxidation: electrons are removed from the chain during the oxidation process, and counterions (dopant) are added to balance the charge allowing neutralization. However, there are still doping processes that do not change the number of electrons in the polymer chain, as in the case of polyaniline (PANI) and its derivatives[10].

The doping processes influence directly on the band structure of the conjugated polymers. The electrical properties of a solid material are a consequence of the electronic band structures, i.e., the arrangement of the outermost electronic bands and the fashion in which they are filled.

Generally, a solid material consists of a large number of atoms that are initially separated from each other, which are subsequently grouped and bonded to form the ordered atomic arrangement. Each atom is independent of all others at relatively large separation distances, presenting an electron configuration and characteristic atomic energy levels. Thus, quantum mechanics states that the electrons of an atom have specific or quantized levels of energy. However, their valence electrons are influenced, or disturbed, by the adjacent electrons and nuclei of atoms. Thus, in the crystalline reticulum, the electronic energy of individual atoms is altered, and each distinct atomic state can be divided into a series of closely spaced electronic states to form the **Energy Band Model**[18]. The band theory allows to understand how the changes in the electronic structure (resulting from the doping process) allow a conductive behavior, as shown in **Figure 3**.

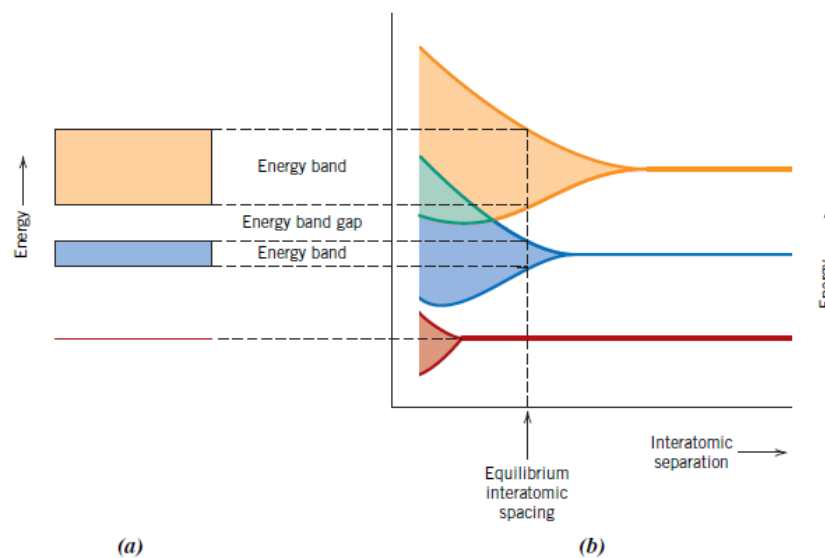


**Figure 3** - (a) Conventional representation of the electronic band energy structure for a solid material at equilibrium interatomic spacing. (b) Electron energy versus interatomic separation for a cluster of atoms[19].



The promotion of the electron to the conduction band allows the electron to be free to move. This process requires sufficient energy supply for the electron to cross the energy gap band and thus fill the empty states located at the bottom of the conduction band[19].

Similar to inorganic semiconductors, conjugated polymers also present an **Energy Gap**,  $E_g$ . This gap separates the energy band of the  $\pi$ -ligand orbitals (presenting all the electronic states occupied) from the  $\pi^*$ -antiligand (presenting all unoccupied states), which are formed due to the conjugation of the polymer chain. According to **Molecular Orbital Theory**, these bands are known as **HOMO (Highest Occupied Molecular Orbital)** and **LUMO (Lowest Unoccupied Molecular Orbital)**, **Figure 4**[20]. The alternation in the distances between the carbon atoms in a conjugated polymer forms one ligand and one antiligand orbital. Thus, four orbitals are formed in the double bond between adjacent carbons: the ligand orbitals  $\sigma$  and  $\pi$ , as well as the antiligand orbitals  $\sigma^*$  and  $\pi^*$ . In the ground state of the  $sp^2$  hybridization, the ligand orbitals are occupied and the antiligand ones are unoccupied[21].

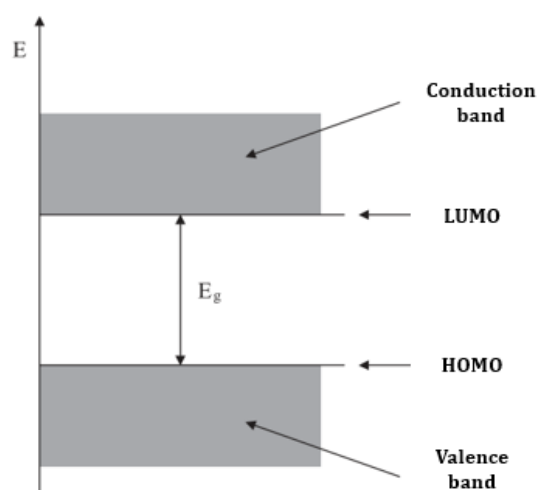


**Figure 4** - Energy diagram of a semiconductor material[20].

For an infinite polymer chain, the coulombian interactions between the  $\pi$ -orbitals results in the delocalization of the electrons along the polymer chain. As a result, an approximately continuous distribution of energy states occurs, creating a distribution of energy bands. The interaction between the  $\pi$ -ligand orbitals (HOMO) resembles the Valence Band (VB) and the interaction between the  $\pi^*$ -antiligand orbitals (LUMO) resembles the Conduction Band (CB), and the difference of energy (HOMO - LUMO) is denoted as  $E_g$ , as shown in **Figure 5**[22].

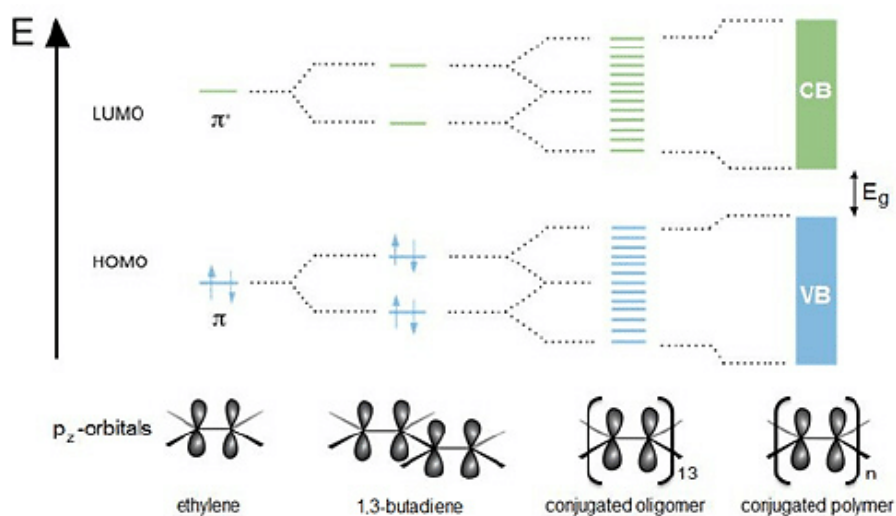


**Figure 5** - HOMO and LUMO bands of conjugated organic molecules [24].

The energy difference between HOMO and LUMO represents the  $E_g$  value of conjugated polymers. Depending on the electronic occupancy and the  $E_g$  value, a solid material is classified as insulator, semiconductor or conductor. Thus, almost all conjugated polymers are classified as semiconductors, presenting  $E_g$  values in the range from 1.5 to 3.2 eV. For comparison, the  $E_g$  values of saturated insulating polymers are greater than 10 eV, which restricts the promotion of electrons from VB to CB band in order to promote electrical conductivity[9].

In conjugated polymers, the doping process represents the mechanism by which the polymer is exposed to oxidizing or reducing agents to effectively convert conjugated polymers to conductive polymers. Doping of conjugated polymers is reversible and therefore the polymer chain is not permanently altered after this process. Due to the doping process, charge centers are generated within the conjugated polymer and the counterion is associated with this charge center in the polymer matrix in order to maintain electroneutrality. Thus, conduction in doped polymers results in the generation and disappearance of charged sites in the conjugated polymer chains, and the electroneutrality of the doped polymer is maintained by incorporation and repulsion of mobile counterions[23].

In their doped, electrically conductive forms, conjugated polymers typically present positive charges (polarons or bipolarons) along their polymer chains, and these charges are balanced by the incorporation of anions. These anions may consist of a variety of chemical groups, such as  $Cl^-$ ,  $HSO_4^-$ ,  $ClO_4^-$ ,  $NO_3^-$  [24], even larger species such as  $(p - TS^-)$  or  $(CSA^-)$ , and large polyelectrolytes and biopolymers[9,10,13].

The oxidation of the conjugated polymer generates a cation radical, or polaron hole, while reduction produces an anion radical, or polaron electron. Polarons allow the appearance of new well-defined energy states within the bandgap, as shown in **Figure 6**[21].

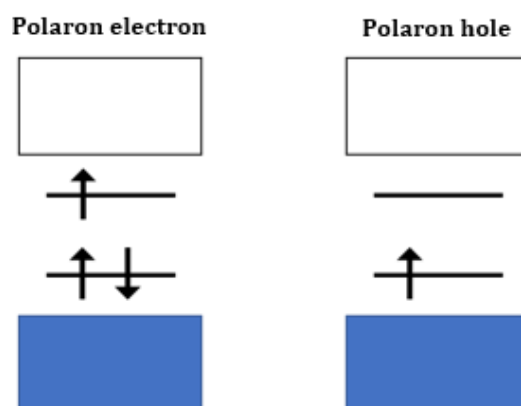


**Figure 6** - Polaron electron and polaron hole band structure.

A cation radical partially delocalized in a polymer segment is known as polaron, presenting spin  $\frac{1}{2}$ . Both radical and cation are coupled to each other by a local resonance. The presence of a polaron induces the creation of a quinone sequence within the polymer chain. The lattice distortion produced is of greater energy than the remaining portion of the chain. The creation and separation of these defects cost energy, which limits the number of quinoid rings that can bond to these two species together. Removal of a second electron results in the bipolaron formation, which is defined as a pair of equal charges (dication with zero spin), associated with strong distortion of the reticule. For conjugated polymers presenting high concentrations of dopants, bipolarons create energy bands symmetrically located above the valence band and below the conduction band. This results in a Fermi energy level close to the maximum (highest energy state) of the valence band, which is partially filled. This is a necessary condition for metal conduction[21].

Theoretical studies show that bipolaron is thermodynamically more stable than two separated polarons due to the coulombic repulsion of two charges confined at the same site and due to the decrease in ionization energy compared to the formation of two polarons. Thus, a bipolaron is a dication forming part of the polymeric structure, presenting positive charges located at a certain site. These charges can occur at many sites in the polymeric structure[25,26]. Thus, excess charges created in the conjugated polymer chains through oxidation or reduction processes are accommodated in electronic states located in the bandgap.

## 2.3 Charge Transport

The charge transport within a doped polymer can be considered as a shift of electrons and holes along the  $\pi$ -conjugated polymer backbone. This ambipolar transport mechanism allows the mobility of charges within the chain (intrachain) and it is associated with the counterion of the doping agent. However, intrachain mobility is not the only mechanism that determines the polymer conductivity. In the absence of any external potential, charge transport can occur by diffusion in all directions.

Thus, charge transport in doped polymers occurs by ***intrachain or intramolecular transport (relocation)***, ***interchain or intermolecular transport (hopping)*** and ***interparticle transport (percolation)***. These processes determine the effective mobility of charge carriers, as shown in **Figure 7**[23].

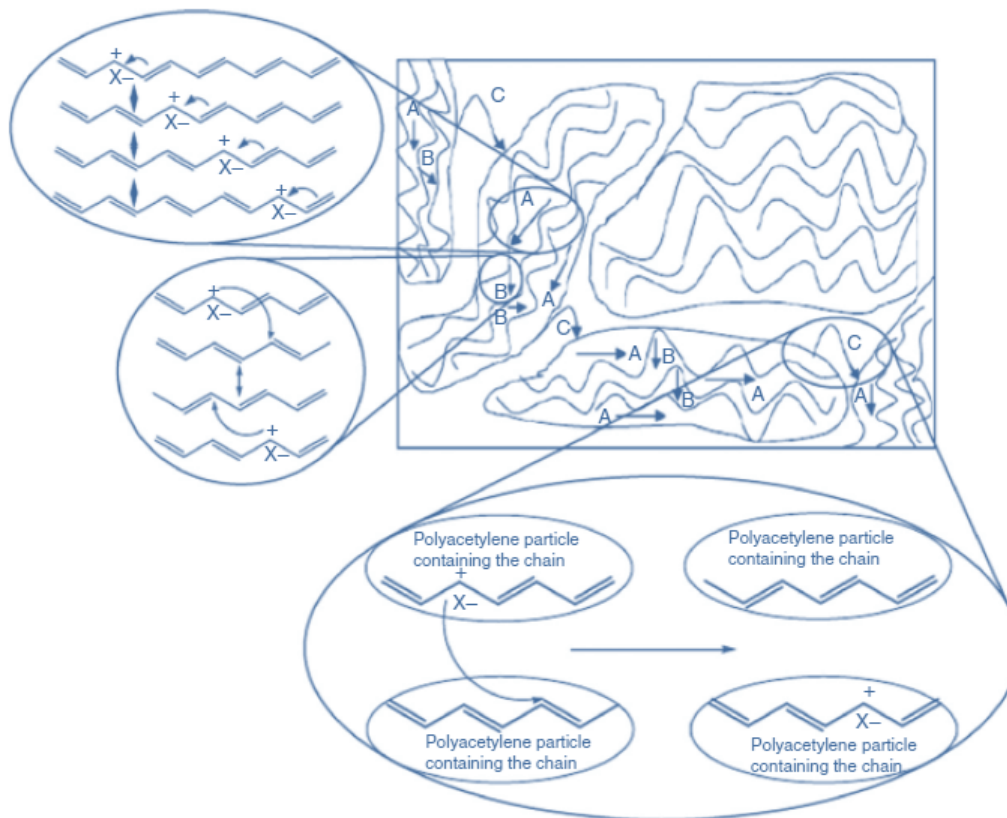


**Figure 7** - Conduction mechanism of doped polymers (a) indicating intrachain charge transport, (b) indicating interchain transport, (c) indicating interparticle transport. Arrows showing the path of the charge carrier migrating through the material.

Conductivity in doped polymers is determined at microscopic (intra and interchain) and macroscopic (interparticle) levels[23]. Hopping is a charge transport mechanism that usually occurs in clustered materials with localized charge carriers. Generally, these regions containing localized charges are known as conducting islands, and may also be associated with regions of high crystallinity, **Figure 8**. Due to the lower rigidity of the polymeric structure, the charge carriers induce a polarization that favors the location of charge carriers. In organic materials, electronic transport occurs mainly through the hopping mechanism. Electrons and holes in a polymer chain jump from one chain to another to carry charges, in contrast to inorganic crystalline solids where band transport is dominant due to the presence of a periodic crystal structure and well-defined state densities[27].

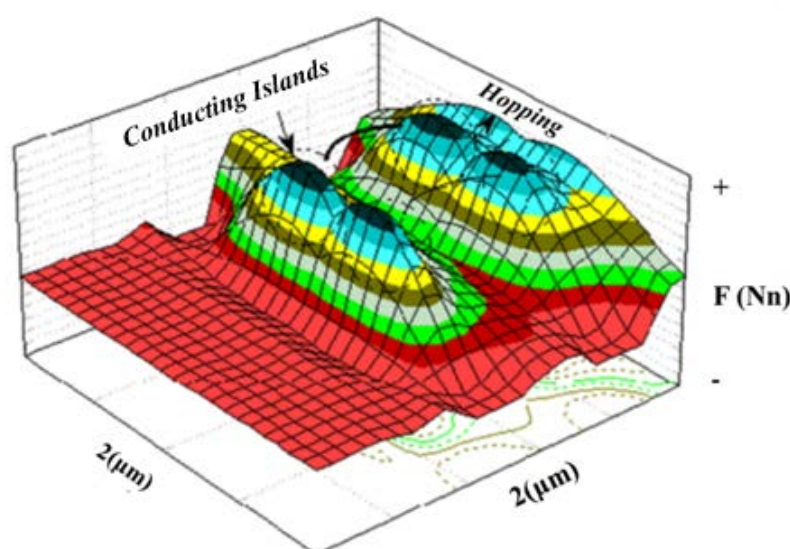


**Figure 8** - Map of forces obtained by Atomic Force Microscopy (AFM) showing conducting islands of poly(*o*-ethoxyaniline) film.

## 2.4 Polyaniline

Polyaniline (PANI) is the product of the aniline oxidative polymerization in acidic medium. It was first reported in 1862, and thereafter studies have been conducted to characterize the synthesis product and its intermediates[28]. The low cost of the monomer, as well as the ease of synthesis and doping makes PANI one of the most interested conjugated polymer in recent years. The chemical synthesis of PANI produces a high purity, molecular weight polymer which can be obtained directly in the doped state in large quantities as a green powder. On the other hand, the electrochemical synthesis has the advantage of the *in situ*

characterization by spectroscopic techniques, as well as the obtainment of the polymer directly in the form of thin films[29,30]. Thermal degradation of doped PANI (Emeraldine-salt form) always occurs above 200 °C[31]. The electrical conductivity of PANI can reach 100 S/cm[32].

The structure of PANI consists of a sequence of benzenoid and quinoid units, as shown in **Figure 9**. Through oxidation and chain reduction, the amount of benzenoid and quinoid units varies and thus different oxidation states are obtained[11].

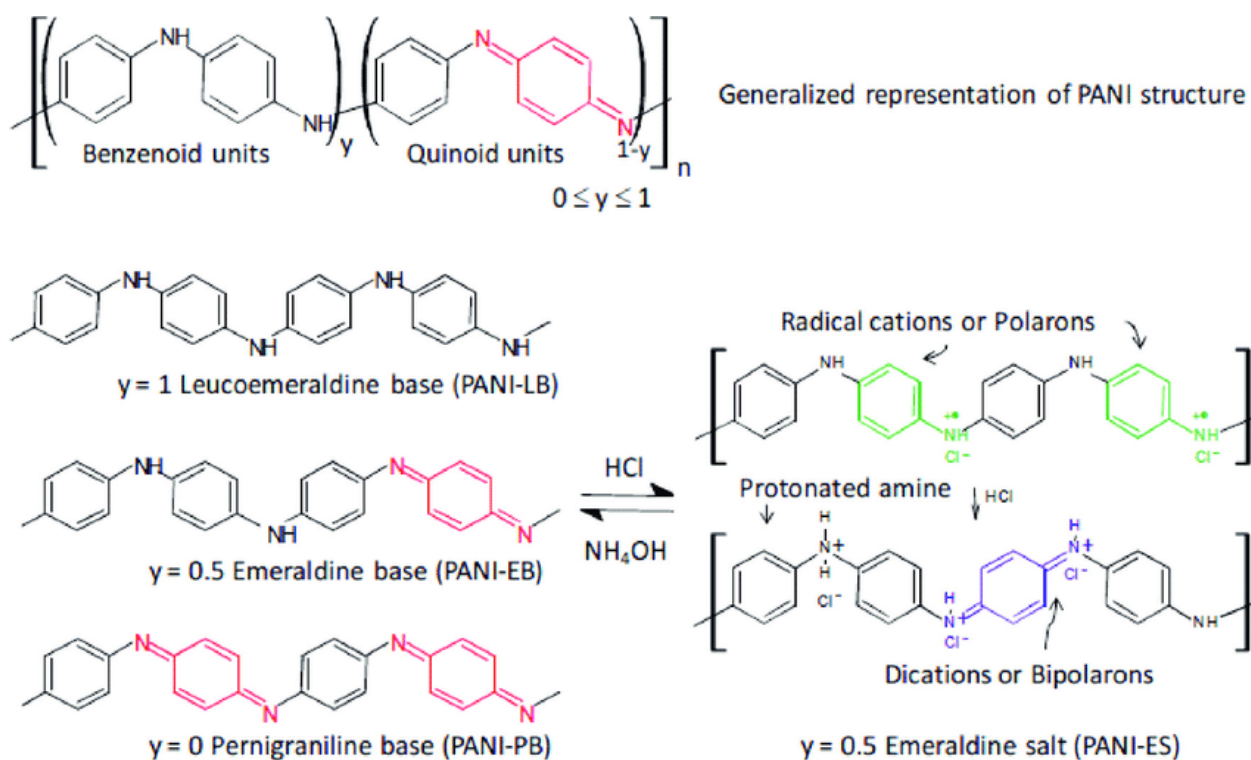


**Figure 9** - Generalized representation of the most common forms of PANI [35].

In its undoped form, PANI is characterized by three distinct oxidation states. Emeraldine-base form (PANI-EB) is the most stable under ambient conditions. PANI oxidation states resulting from the PANI-EB reduction and oxidation are the leucoemeraldine-base form (PANI-LB) and pernigraniline-base form (PANI-PB), respectively. The LB state is colorless or yellow in aerobic ambient and tends to light green as it oxidizes, while the PB state is violet. The unique characteristics of PANI arise from exposure of its EB state to strong acids. This induces the formation of its emeraldine-salt form (PANI-ES), which exhibits an electrical conductivity that increases by about 10 orders of magnitude[33].

In contrast to *p* and *n*-type of doping processes applied to other conjugated polymers such as polyethylene, polypyrrole, polythiophene etc., PANI-EB is doped by a protonation process with no addition or electron removal from the structure to form the conduction state[34]. Mainly through the protonation of the nitrogen imine, the formation of charged



segments such as cation radicals (polarons) and dications (bipolarons) within the polymeric structure is observed[35].

Oxidation and/or reduction reactions occur during the polymer doping process, and the counterion (dopant) remains in the polymer matrix. PANI-EB,  $y = 0.5$ , is the first successful example of doped polymer that has resulted in a highly conductive regime through a process in which the number of electrons remains unchanged (protonation), and this process is related to its acid-base properties[9].

The protonation of PANI-EB (blue – undoped form) using 0.1M HCl produces a 10-order increase in conductivity leading to the formation of PANI-ES (green - doped form). The imine nitrogen may be wholly or partially protonated to obtain the polymer in the salt form, i.e., in the doped form. Deprotonation occurs reversibly by similar treatment using basic aqueous [9].

PANI can be synthesized in the powder form using a suitable oxidizing agent, or in the form of thin films by electrochemical oxidation of the monomer electrodes on different inert materials[36].

The chemical polymerization of aniline in aqueous solution was studied as a function of a variety of synthesis parameters, such as pH, reagent concentration, different oxidizing agents and protonic acids, temperature and polymerization time. The main parameters that affect the polymerization process and the properties of the final product are basically summarized in the nature of the oxidizing agent, the nature of the dopant acid and the temperature of the reaction medium [37,38].

## 2.5 Poly(*o*-methoxyaniline)

A number of reports on the synthesis of PANI derivatives have been conducted to increase solubility and maintain electrical properties at acceptable levels. The introduction of long functional and flexible polar functional groups and alkyl groups, linked mainly to the polymer main chain, represents an alternative to obtain soluble polymers in a larger variety of organic solvents, which facilitates their characterization and processability[39].

PANI-ES is insoluble in most organic solvents and also infusible, which difficulties its industrial application. The insolubility of PANI-ES can be attributed to the rigidity of its main chain, resulting from the strongly  $\pi$ -conjugated system. Electron-donating substituent groups at the positions 2 and 5 of the ring cause distortion in the main chain, reducing its conjugation



and making it more flexible. As a result, there is increased solubility and decreased electrical conductivity[40].

Several methodologies have been proposed to solve the problems of processability, solubility and electrical conductivity. The incorporation of polar functional groups or long, flexible chains into the polymeric structure represents a common technique for preparing water-soluble polymers or organic solvents. Recent studies with substituted polyanilines show the importance of investigating the influence of substituent groups on polymer properties[41].

Some studies have been developed to produce PANI derivatives without compromising their electrical properties, showing that PANI processability is improved when using alkyl and alkoxy substituents in the ring, such as  $-\text{CH}_3$ ,  $-\text{OCH}_3$ ,  $-\text{SO}_3\text{H}$  and  $-\text{OCH}_2\text{CH}_3$ . The preparation of derivatives involves the same methods used for aniline polymerization[40,42]. Poly(*o*-methoxyaniline) (POMA), poly(*o*-ethoxyaniline) (POEA) and sulfonated PANI represent the most common PANI derivatives.

POMA is a derivative from PANI whose structural difference lies in the presence of a methoxy group ( $-\text{OCH}_3$ ) at the *ortho* position of the carbon rings[43], **Figure 10**. Despite the structural similarity and similar physical properties of PANI, POMA has improved solubility due to the incorporation of flexible groups in the chain structure (inducing a torsion in the structure with modification of the planarity effect)[2].

POMA can also be obtained in different oxidation states., such as emeraldine-base and salt forms. The conversion from base to salt form can be achieved via protonation in acid medium[10].

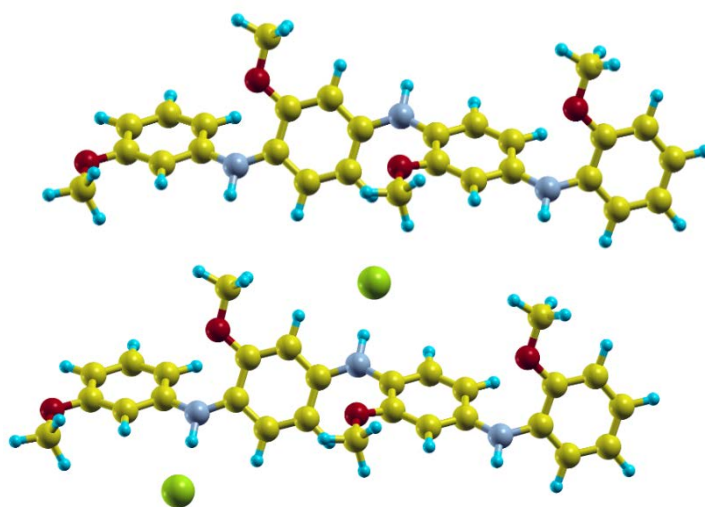


**Figure 10** - Molecular structure of a POMA tetramer as (a) Emeraldine-base (POMA-EB) and (b) Emeraldine-salt (POMA-ES) forms.

POMA has been widely studied in the form of powder obtained by chemical synthesis or in the form of films obtained by electrochemical synthesis, allowing many technological applications. In 1988, Macinnes and Funt described the preparation of POMA by oxidizing the monomer with  $(\text{NH}_4)_2\text{S}_2\text{O}_8$  and HCl. The authors obtained a soluble polymer in DMF, acetic acid and sulfuric acid. The product presented electroactivity and electrical conductivity of 3 S/cm. POMA also presented similar properties when electrochemically prepared[40].

## 2.6 Influence of Dopant Acids on the Properties of Conjugated Polymers

The role of the doping process is to improve the electrical conductivity of the polymer. Doping of conjugated polymers results in significant changes in electrical, magnetic, optical and structural properties. Generally, counterions are simultaneously inserted into the conjugated polymer matrix. Thus, doped polymers are considered to be polymeric organic salts. Reducing or oxidizing agents, which convert the polymer to polymeric salts, are known as "doping agents" or "dopants". Therefore, doping of a conjugated polymer refers to the addition of an electron donor/acceptor molecule, as well as a protonating agent to the polymer[7]. **Figure 11** compares the electrical conductivity of different types of materials.

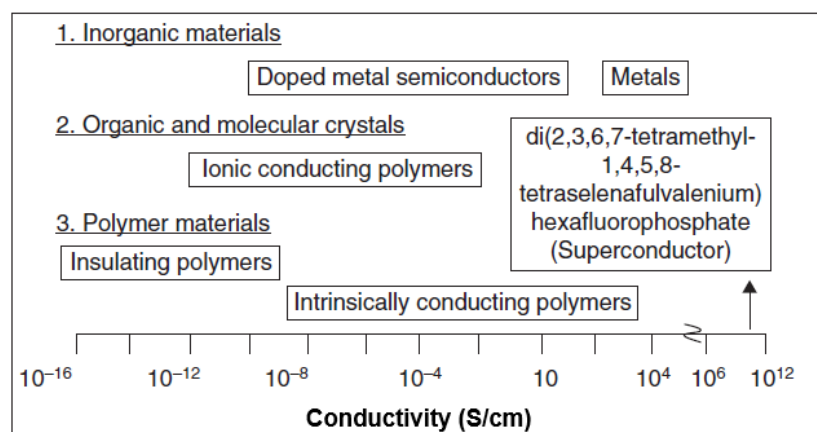


**Figure 11** - Electrical conductivity (S/cm) of materials[23].

The doping process enhances the electrical properties of the polymer, and its application as semiconductor becomes feasible in a competitive way with metals. The change of these properties can be observed in several analyzes. Starting with FTIR, peak displacements can be observed when comparing doped and undoped polymers. Due to the extended electronic conjugation, which decreases the strength of bonds in conjugated polymers, the position of the corresponding vibrations changes to shorter wavelengths[44].

Temperature also influences the properties of conjugated polymers, such as electrical conductivity. The temperature-dependent electrical conductivity of doped polymers is similar to inorganic semiconductors but different from metallic ones[45].

DRX technique allows to verify the structural effects of the doping process on various conductive polymers. Doping also leads to different forms of crystalline regions that differ from undoped polymers[46]. A detailed study of PANI has shown that an increase in crystallite size was observed, besides a decrease in interchain separation after doping[45].

The processability is also influenced by the doping process. The use of dopant acids with larger counterions improves the processability of the doped polymer. However, its electrical conductivity is decreased[47].

## 2.7 Applications of Conjugated Polymers

Conjugated polymers present a large number of applications such as supercapacitors, light emitting diodes (LEDs), field effect transistors (FETs), solar cells, actuators and biosensors, among others[48].

Chemical sensors are one of the main applications of conjugated polymers. They form a selective layer in which, through the interaction between the analyte and the conductive matrix, changes in the physical parameters of the polymer can be used in the transduction mechanism [49]. Most conductive polymers have been tested as gas sensor[50–52]. In  $\pi$ -conjugated systems, the interaction between organic materials and gas molecules results in the increase/decrease of polaron/bipolaron density within the bandgap. Since polaron and bipolaron excitations generally are present within the visible radiation range, their population changes imply both in electrical and optical changes[53].

Polymeric chains can be exemplified as motors due to their changes in length (conformational movements) during the oxidation and reduction process. The coiled of these molecular motors expands or shrinks under electrochemical stimulation of the electroactive parts of the chains. The result is an isotropic three-dimensional change in volume producing mechanical properties[54]. Biomimetic systems based on the combination of a tri-layer polymer have been proposed for swimming devices, where wave motion is employed to create sufficient thrust for propulsion[55]. Other applications such as swiveling microcatheters[56], micropumps[57], and microactuators[58] have being studied.

Conductive polymers are promising materials for organic-inorganic hybrid composites for Li-ion batteries due to their excellent features including high chromic efficiency and electrical conductivity. Conductive polymers exhibit several advantages such as low cost, convenient molecular modifications and low weight for application as electrodes[59,60].

Due to their flexible structure, organic polymers can absorb larger Na<sup>+</sup> ions reversibly without many spatial problems, helping to achieve rapid kinetics for Na<sup>+</sup> insertion and extraction reactions. A Na-ion battery can be designed by using an organic cathode and anode pair that always have sufficient potential difference and can be well coupled to perform a battery reaction. An all-organic Na-ion battery would be very attractive for large-scale electrical storage applications because of its low cost and eco-friendliness[61].

Biosensors are analytical devices used to detect specific analytes. A biosensor is typically composed of a biological sensor element and a transducer[62]. The biological sensing elements may be enzymes, antibodies, cell receptors or DNA. The transducer may be a piezoelectric, optical or physicochemical material that translates biological signals into electrical and optical signals[63]. By incorporating different biological sensing elements into the conducting polymer, the biosensors can detect various types of biological materials. As an example we have the manufacture of a carbon nanotube and polypyrrole composite for glucose detection[64] and DNA sensors for applications in forensic investigations, drug discovery and diagnostic methods[48]. Immunosensors are extremely useful tools for environmental monitoring, food quality screening and disease control, and are based on the detection of specific antigens[65]. Antigens can be defined as foreign molecules that lead to antibody production by the immune system[48].

## 3 EXPERIMENTAL

### 3.1 Polymer Synthesis

Conventional oxidative polymerization of *o*-methoxyaniline was based on the method described by Sanches et al.[66] and Bhadra et al.[67] with slight modifications. Solution A was prepared at 25 °C by solubilizing 28 mL of *o*-methoxyaniline in 300 mL of HCl, HNO<sub>3</sub>, H<sub>2</sub>SO<sub>4</sub> or H<sub>3</sub>PO<sub>4</sub>, 2 M. Solution B was obtained by adding 11.6 g of ammonium persulfate (APS) in the same acid solution (200 mL, 2 M). Solution B was added drop by drop to solution A. The system remained under constant stirring for 3 h. Then, the obtained polymers POMA/HCl, POMA/HNO<sub>3</sub>, POMA/H<sub>2</sub>SO<sub>4</sub> or POMA/H<sub>3</sub>PO<sub>4</sub> were vacuum filtered and maintained at desiccator until reach constant weight.

### 3.2 XRD Analysis and Percentage of Crystallinity

XRD data were obtained at the Laboratório de Materiais (LabMat – UFAM) on a Panalytical diffractometer, Empyrean model, operating with CuK $\alpha$ , 40 kV and 40 mA. XRD patterns were collected in the range  $2\theta = 5 - 70^\circ$ , step of  $0.013^\circ$  and 5 s/step. Percentage of crystallinity was assessed by the ratio between the peak areas to the area of the non-crystalline broad halo contribution.

### 3.3 Le Bail Method

The software package Fullprof[68] was used to perform the Le Bail method[8]. The least squares method[69] was applied to refine all parameters. The peak profile was adjusted according to the *pseudo*-Voigt function modified by Thompson-Cox-Hastings[70]. A LaB<sub>6</sub> crystal standard was used to obtain the instrumental resolution function parameters. Crystal data from the end-capped tetramer of aniline[71] were considered as initial parameters (triclinic,  $P\bar{1}$ ;  $a = 5.7328 \text{ \AA}$ ;  $b = 8.8866 \text{ \AA}$ ;  $c = 22.6889 \text{ \AA}$ ;  $\alpha = 82.7481^\circ$ ;  $\beta = 84.5281^\circ$  and  $\gamma = 88.4739^\circ$ ). Crystallite anisotropy was evaluated using linear combination of spherical harmonics (SHP)[72].

### **3.4 SEM Analysis**

Scanning Electron Microscopy (SEM) experiments were performed in a Carl Zeiss equipment, model Supra 35, using 1.0 kV at 25 °C. Polymers were placed on a carbon tape and recovered with a thin gold layer prior to analysis.

### **3.5 Fourier-transform Infrared Spectroscopy (FTIR) Analysis**

Measurements were carried out using a spectrophotometer Thermo Scientific, Model Nicolet iS10, in the range of 400 – 1800  $\text{cm}^{-1}$ . Polymer pellets were prepared with KBr (1:100 w/w).

### **3.6 Thermogravimetric Analysis (TG/dTG)**

TG/dTG analysis was performed in a Shimadzu 60 equipment. Measurements were performed from 27 – 800 °C under  $\text{N}_2$  atmosphere (flow of 50 mL/min) and heating rate of 10 °C/min.

### **3.7 Complex Impedance Spectroscopy analysis (CIS)**

A Solartron 1260 impedance analyzer was used for collecting data at room temperature.

## 4 RESULTS AND DISCUSSION

### 4.1 X-ray Diffraction Analysis and Percentage of Crystallinity

**Figure 12(a)** shows the diffractograms of the polymers POMA/HCl, POMA/HNO<sub>3</sub>, POMA/H<sub>2</sub>SO<sub>4</sub> and POMA/H<sub>3</sub>PO<sub>4</sub>. **Figure 12(b)** highlights the most intense diffraction peaks in the angular region  $2\theta = 5 - 30^\circ$ . Peak broadening is related both to the polymer crystallinity and crystallite size. In fact, the lower intense, less defined diffraction peaks were observed in the POMA/H<sub>3</sub>PO<sub>4</sub> pattern probably due to the chemical nature of this doping acid.

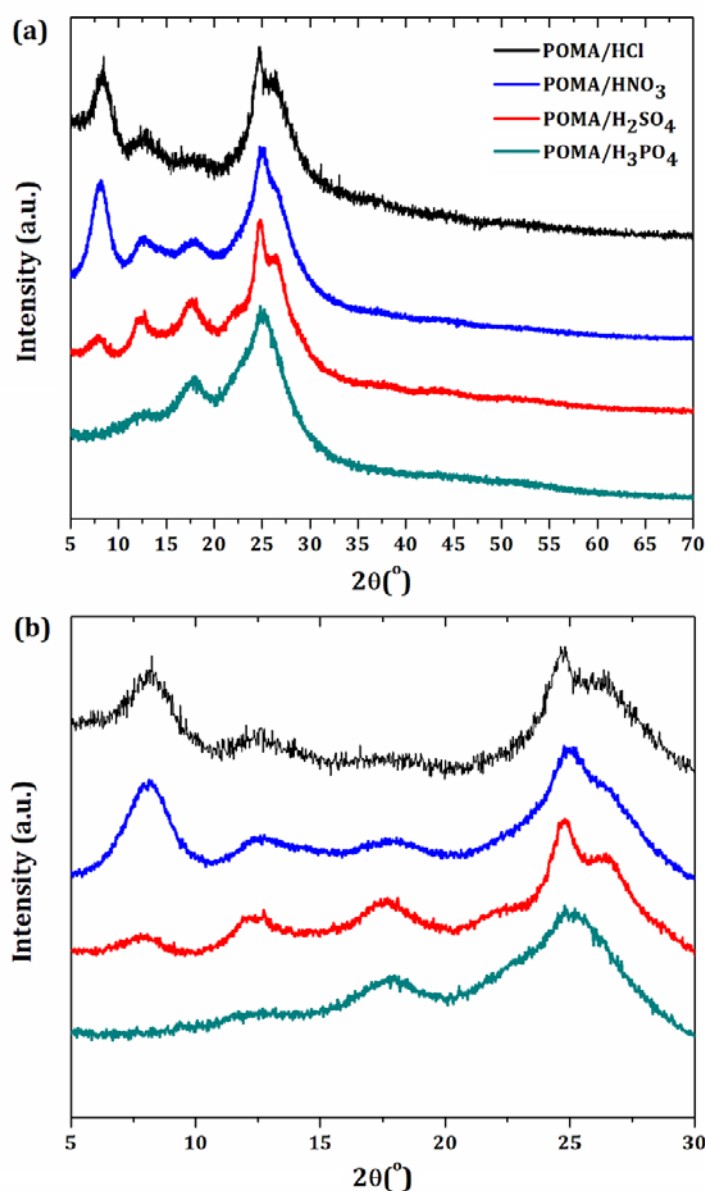


**Figure 12** - (a) X-ray diffraction patterns of the polymers POMA/HCl, POMA/HNO<sub>3</sub>, POMA/H<sub>2</sub>SO<sub>4</sub> and POMA/H<sub>3</sub>PO<sub>4</sub> and (b) the angular region  $2\theta = 5 - 30^\circ$  highlighting the most intense diffraction peaks.



The first diffraction peak did not present good resolution and intensity in the XRD pattern of the polymer POMA/H<sub>3</sub>PO<sub>4</sub>. It is known that the doping acids HCl, HNO<sub>3</sub> or H<sub>2</sub>SO<sub>4</sub> have almost complete chemical dissociation,  $pK_a < 1$ . For this reason, their resulting doping process were more efficient when compared to that of H<sub>3</sub>PO<sub>4</sub>, a weak acid with  $pK_a = 2.12$ . This fact can be verified by the resulting percentage of crystallinity, which will be discussed later. For this reason, the doping acid influenced on the polymer crystallinity[73,74], so the semi crystalline XRD patterns of the as-synthesized polymers is a consequence of some polymer chain alignment. However, broad peaks are due to the nanosized crystalline phase (crystallites), which coexist with the non-crystalline one.

Angular displacements of diffraction peaks are associated to changes in lattice parameters. **Figure 13** shows the peak deconvolution of the polymers POMA/HCl, POMA/HNO<sub>3</sub>, POMA/H<sub>2</sub>SO<sub>4</sub> and POMA/H<sub>3</sub>PO<sub>4</sub>. In order to assess the peak position accurately, the experimental XRD patterns (black curves) were fitted (red curves) by using the Gaussian function (green curves). The blue curves are due to the non-crystalline contribution. According to **Table 1**, the diffraction peak positions were considerably influenced by the counterion sizes. The deconvolution method allowed to observe slightly peak displacements to lower angles in the polymers POMA/HNO<sub>3</sub>, POMA/H<sub>2</sub>SO<sub>4</sub> and POMA/H<sub>3</sub>PO<sub>4</sub> when compared to those of POMA/HCl polymer. Angular displacements of diffraction peaks are associated to changes in lattice parameters. The XRD patterns of the polymers synthesized with doping acids of larger counterions, such as HNO<sub>3</sub>, H<sub>2</sub>SO<sub>4</sub> or H<sub>3</sub>PO<sub>4</sub>, presented peaks located at slightly smaller angular positions. Due to the presence of the counterions along the polymeric chains in order to guarantee electroneutrality, the unit cell parameters, cell volumes, as well as angular positions ( $d$ -spacing) were modified. Diffraction peak displacements of conjugated polymers due to the presence of counterions have been reported in scientific literature[75]. However, no up to date reports of poly(*o*-methoxyaniline) have been found.

Despite observing slightly differences in the XRD patterns, the ratio between the areas of the diffraction peaks to the area of the non-crystalline contribution was similar for the polymers POMA/HCl, POMA/HNO<sub>3</sub> and POMA/H<sub>2</sub>SO<sub>4</sub>, which was estimated to be  $(50 \pm 2)$  %. On the other hand, the polymer POMA/H<sub>3</sub>PO<sub>4</sub> presented the lowest percentage of crystallinity, estimated around  $(40 \pm 1)$  %. The different degree of crystallinity was attributed to the strength of the dopant acids and, consequently, to their ability of chemical dissociation and doping, resulting in the alignment of the polymer chains.

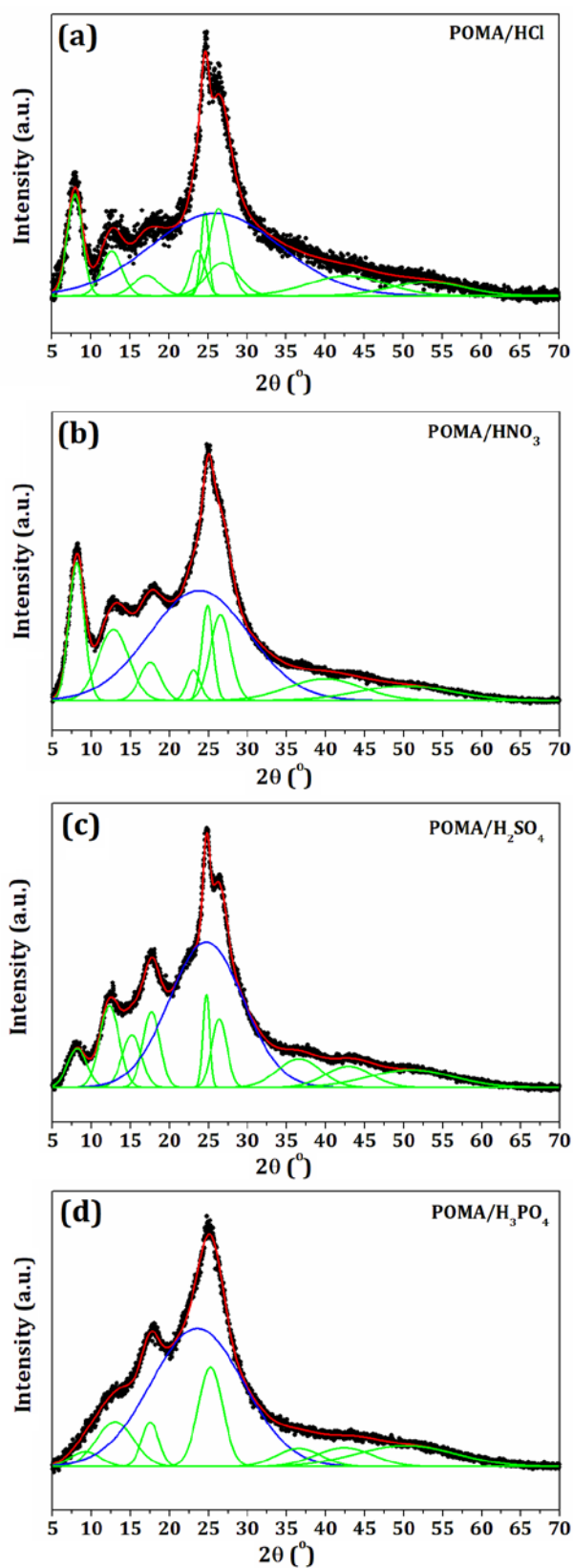


**Figure 13** - Peak deconvolution of the polymers (a)POMA/HCl, (b)POMA/HNO<sub>3</sub>, (c)POMA/H<sub>2</sub>SO<sub>4</sub> and (d)POMA/H<sub>3</sub>PO<sub>4</sub>. XRD patterns (black curves) were fitted (red curves) by using the Gaussian function (green curves). The blue curves are due to the non-crystalline contribution.

**Table 1** - Diffraction peak positions ( $2\theta$ ) of POMA/HCl, POMA/HNO<sub>3</sub>, POMA/H<sub>2</sub>SO<sub>4</sub> and POMA/H<sub>3</sub>PO<sub>4</sub>.

POMA/HCl	POMA/HNO <sub>3</sub>	POMA/H <sub>2</sub> SO <sub>4</sub>	POMA/H <sub>3</sub> PO <sub>4</sub>
$2\theta$ (°)	$2\theta$ (°)	$2\theta$ (°)	$2\theta$ (°)
(8.00 ± 0.01)	(7.81 ± 0.01)	(7.62 ± 0.01)	-
(12.81 ± 0.01)	(12.51 ± 0.01)	(11.92 ± 0.01)	(11.61 ± 0.01)
(17.94 ± 0.01)	(18.12 ± 0.01)	(17.44 ± 0.01)	(17.25 ± 0.01)
(24.93 ± 0.01)	(24.84 ± 0.01)	(24.63 ± 0.01)	(24.43 ± 0.01)
(26.47 ± 0.01)	(26.23 ± 0.01)	(26.02 ± 0.01)	-

## 4.2 Le Bail Method

The structural refinement through the Le Bail Method[8] was performed to obtain cell parameters, as well as crystallite size and shape of the as-synthesized polymers. **Table 2** shows the refined parameters, as well as the crystal data used as initial parameters[71]. The lattice parameters along [001] direction remained almost similar in all polymers; however, a considerable difference around 4 Å was found when compared to the initial parameters. This fact is due to the absence of the phenyl-end-capped group in the as-synthesized polymers.

The refined cell parameters “c” were found from 17.93 Å – 18.99 Å, suggesting that the polymers POMA/HCl, POMA/HNO<sub>3</sub>, POMA/H<sub>2</sub>SO<sub>4</sub> and POMA/H<sub>3</sub>PO<sub>4</sub> presented four repetitive units per unit cell (tetrameric molecules), which may be arranged along [001]. The unit cell parameters along [100] and [010] directions were considerably influenced by the presence of counterions. These results were explained by the incorporation of the counterions along the polymeric chains to guarantee electroneutrality after doping process. The cell parameters “b” presented larger values for those polymers synthesized with larger counterions: 11.986 Å, 11.942 Å, 12.227 Å and 12.229 Å were found for the polymers POMA/HCl, POMA/HNO<sub>3</sub>, POMA/H<sub>2</sub>SO<sub>4</sub>, and POMA/H<sub>3</sub>PO<sub>4</sub>, respectively. Moreover, the polymers presenting the largest counterions (POMA/H<sub>2</sub>SO<sub>4</sub> and POMA/H<sub>3</sub>PO<sub>4</sub>) consequently presented larger unit cell volume (2,066 Å<sup>3</sup> and 2,057 Å<sup>3</sup>, respectively).

The influence of counterions on the unit cell dimensions of conjugated polymers have been reported[76–78]. However, no reports have been found for poly(*o*-methoxyaniline) considering different dopant acids. The counterion Cl<sup>-</sup> influenced on the unit cell parameter “b”

of the emeraldine-salt form of polyaniline (PANI-ES)[5]. The authors reported a double value along [010] ( $b = 18.5 \text{ \AA}$ ) when compared to the initial crystal data[71]. These results also suggested the incorporation of this counterion in the molecular structure of PANI. The influence of the counterion  $\text{Cl}^-$  was also verified along [010] direction when PANI was doped to obtain PANI-ES, as well as when it was synthesized in the presence of  $\text{CeO}_2$  to form a core-shell nanocomposite[79].

**Table 2** - Le Bail method performed for the polymers POMA/HCl, POMA/ $\text{HNO}_3$ , POMA/ $\text{H}_2\text{SO}_4$  and POMA/ $\text{H}_3\text{PO}_4$  using the program Fullprof: lattice parameters, unit cell volume, crystallite average size, and agreement factors ( $R_{wp}$ ,  $R_p$  and  $\chi^2$ ).

Refined Parameters	Initial Parameters [72]	POMA/HCl	POMA/ $\text{HNO}_3$	POMA/ $\text{H}_2\text{SO}_4$	POMA/ $\text{H}_3\text{PO}_4$
$a$ ( $\text{\AA}$ )	5.7328	6.0233 (2)	7.0138 (2)	9.0173 (2)	8.9773 (2)
$b$ ( $\text{\AA}$ )	8.8866	11.9863 (2)	11.9429 (2)	12.2276 (2)	12.2294 (2)
$c$ ( $\text{\AA}$ )	22.6889	18.9307 (2)	17.9374 (2)	18.9928 (2)	18.9710 (2)
$\alpha$ ( $^\circ$ )	82.7481	83.1724 (2)	82.5956 (2)	82.8733 (2)	82.8257 (2)
$\beta$ ( $^\circ$ )	84.5281	84.1401 (2)	84.3640 (2)	84.0366(2)	84.4921 (2)
$\gamma$ ( $^\circ$ )	88.4739	88.8810 (2)	88.3522 (2)	88.2290 (2)	88.5701 (2)
Crystallite Average Size ( $\text{\AA}$ )	-	(46 $\pm$ 2)	(43 $\pm$ 2)	(48 $\pm$ 2)	(44 $\pm$ 2)
Crystallite Size [100] ( $\text{\AA}$ )	-	66	47	66	60
Crystallite Size [010] ( $\text{\AA}$ )	-	37	43	29	35
Crystallite Size [001] ( $\text{\AA}$ )	-	36	39	55	46
Unit Cell Volume ( $\text{\AA}^3$ )	1141	1350	1483	2066	2057
$R_{wp}$	11.3	10.2	4.38	4.03	5.06
$R_p$	4.9	7.15	2.99	2.88	3.07
$\chi^2$	1.54	2.04	2.09	1.5	2.17

The Le Bail method also allowed the obtainment of crystallite size and shape. According to **Table 2**, the largest crystallite size was found along [100] direction. In contrast, the smallest size was expected to be found along the larger lattice parameter, [001]. The crystallite average size did not present significant difference as a function of the doping acid, ranging from 43  $\text{\AA}$  – 48  $\text{\AA}$ . Although the percentage of crystallinity was clearly found in two distinct values (50 % or 40 %), they are not directly related to the average crystallite sizes. Considering the deviations, all polymers presented similar crystallite average size. Larger average crystallite size was expected for POMA/HCl due to the strength doping acid and also to the smaller size of the  $\text{Cl}^-$  counterion, favoring the polymer chains alignment. However, this fact was not observed. Moreover, crystallites seemed to reach a maximum average size, independently of the percentage of crystallinity or the nature of the counterion.

Previous reports based on PANI and its derivatives also verified average crystallite size smaller than 55 Å[5,80,81]. The HCl-doped POMA was previously synthesized[5] from 0.5 to 72 h. The maximum crystallite size was reported around 55 Å. Crystallite size of PANI (synthesized for 3 h using HCl 1M) was found around 38 Å. Another work reporting the poly(*o*-ethoxyaniline) (POEA) doped using HCl presented crystallite size of 26 Å. PANI-ES presented crystallite size around 41 Å even when synthesized with Al<sub>2</sub>O<sub>3</sub> in the form of a highly conducting nanocomposite[82]. Thus, no average crystallite size larger than 55 Å were found for PANI nor its derivatives, suggesting that it may be a limited size of these conjugated polymers. The 2D-images of crystallites along [100], [010] and [001] directions are shown in **Figure 14**.

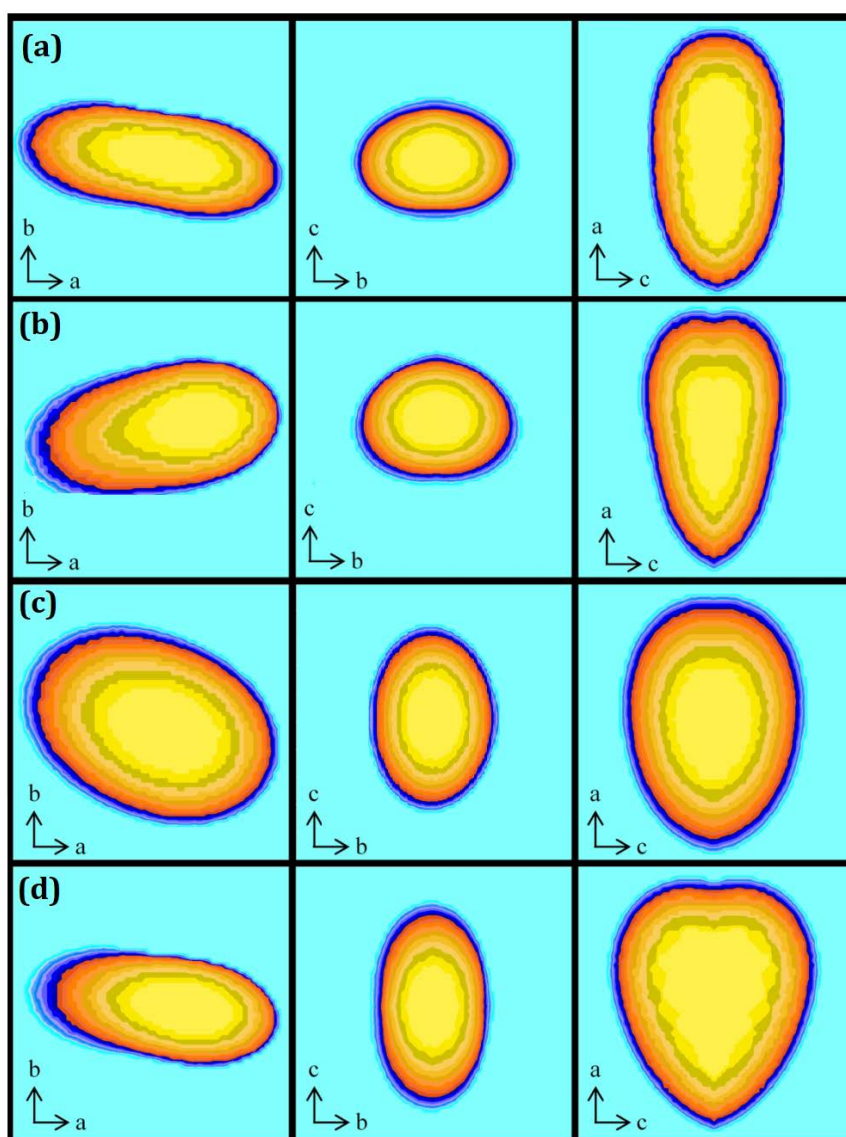


**Figure 14** - Crystallite shape projections for the polymers (a) POMA/HCl, (b) POMA/HNO<sub>3</sub>, (c) POMA/H<sub>2</sub>SO<sub>4</sub> and (d) POMA/H<sub>3</sub>PO<sub>4</sub> along [100], [010] and [001].

The as-synthesized polymers presented a prolate-like crystallite shape. The smaller growth plane of POMA/HCl and POMA/HNO<sub>3</sub> was the [001] direction, as shown in **Table 2**. However, the polymers POMA/H<sub>2</sub>SO<sub>4</sub> and POMA/H<sub>3</sub>PO<sub>4</sub> presented the smaller growth planes exactly along [010] direction, suggesting a considerable difficult of chain packing along this direction.

The polymers POMA/HCl and POMA/HNO<sub>3</sub> presented equal growth planes possibly due to their almost similar counterion size. For this reason, the chains tended to be aligned in parallel, since the small size of the counterion does not significantly influence on the chain packaging, so the crystallites are larger along [100] direction.

The crystallites of the polymers POMA/H<sub>2</sub>SO<sub>4</sub> and POMA/H<sub>3</sub>PO<sub>4</sub> presented considerable growth along [100] and [001] directions, and marginal growth over [010] direction. The smaller crystallite size along [010] direction is due to the larger counterions that affect the chain packing. These observations can be visualized in the 2D-images of crystallites: the smaller size was observed along [001] direction for the polymers POMA/HCl and POMA/HNO<sub>3</sub>, and along [010] direction for POMA/H<sub>2</sub>SO<sub>4</sub> and POMA/H<sub>3</sub>PO<sub>4</sub>. This fact may be explained by the influence of their respective counterions on the polymer chain packing.

### 4.3 FTIR Analysis

The FTIR absorption bands of the as-synthesized polymers are shown in **Figure 15**. For conjugated systems and alkenes, the band related to the C=C stretching appears around 1,625 cm<sup>-1</sup>; however, in asymmetric conjugated diene spectra it is located from 1,650 cm<sup>-1</sup> to 1,600 cm<sup>-1</sup>. For this reason, the band located at 1,649 cm<sup>-1</sup> (**1**) was assigned to the C=C stretching[83]. The C-H angular deformation of the group -OCH<sub>3</sub>[84–86] was observed at 1,460 cm<sup>-1</sup> (**2**). The C-N stretching was found at 1,290 cm<sup>-1</sup> (**3**)[87] since this band has been reported as a strong absorption between 1,342 cm<sup>-1</sup> and 1,266 cm<sup>-1</sup>[83]. The band at 1,255 cm<sup>-1</sup> (**4**) was assigned to the C-O-C stretching of alkyl aryl ether[86]. The 1,4-substituted benzene ring occurred at 1,203 cm<sup>-1</sup>, 1,119 cm<sup>-1</sup>, 1,014 cm<sup>-1</sup> and 793 cm<sup>-1</sup> (**5**). The out-of-plane C-H deformation of mono and 1,2-disubstituted carbon was observed at 746 cm<sup>-1</sup> (**6**)[87]. The band at 831 cm<sup>-1</sup> (**7**), which was assigned to the out-of-plane C-H deformation of benzenoid rings[88], was observed in all polymers. However, this band presented lower intensity in the POMA/H<sub>3</sub>PO<sub>4</sub> spectrum. The band at 600 cm<sup>-1</sup> (**8**) was assigned to the C-H angular deformation of methoxy group[89]. The band at 590 cm<sup>-1</sup> (**9**) was attributed to the counterion HSO<sub>4</sub><sup>-</sup> [90] in the POMA/H<sub>2</sub>SO<sub>4</sub> spectrum.

The band at  $1,171\text{ cm}^{-1}$  (**10**) presented a shift to  $1,182\text{ cm}^{-1}$  (**11**) in the POMA/ $\text{H}_2\text{SO}_4$  spectrum due to the asymmetric stretching of  $\text{S}=\text{O}$ . The in-plane C-H vibration mode of the quinoid rings was observed at  $960\text{ cm}^{-1}$  (**12**) [86]. A particular band observed at  $1,385\text{ cm}^{-1}$  (**13**) in the POMA/ $\text{HNO}_3$  spectrum was assigned to the symmetric axial deformation of  $\text{NO}_2$  [83].

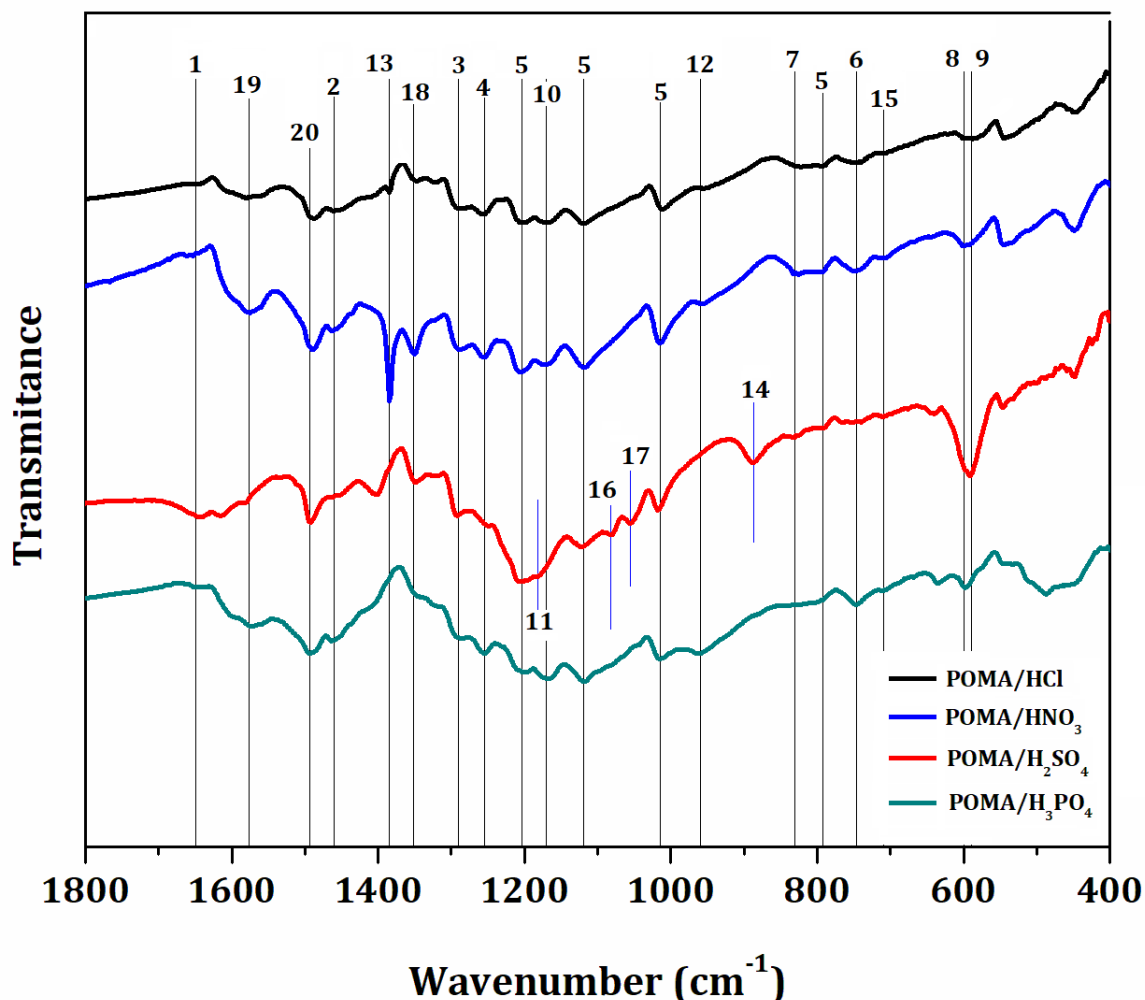


**Figure 15** - FTIR spectra of the polymers POMA/ $\text{HCl}$ , POMA/ $\text{HNO}_3$ , POMA/ $\text{H}_2\text{SO}_4$  and POMA/ $\text{H}_3\text{PO}_4$ .

Another particular band was located at  $887\text{ cm}^{-1}$  (**14**) and attributed to the molecular counterions  $\text{HSO}_4^-$ . The  $\text{S}-\text{O}$  stretching vibration was found at  $710\text{ cm}^{-1}$  (**15**), and  $\text{SO}_3^-$  at  $1082\text{ cm}^{-1}$  (**16**) and  $1055\text{ cm}^{-1}$  (**17**). Bands possibly due to residual APS were located at  $1,352\text{ cm}^{-1}$  (**18**). The oxidation of PANI by APS results in byproducts such as  $\text{H}_2\text{SO}_4$  and  $(\text{NH}_4)_2\text{SO}_4$  [90], which was confirmed by the  $\text{S}(\text{=O})_2$  asymmetric stretching [83].

The absorption bands of  $\text{N}=\text{Q}=\text{N}$  and  $\text{N}-\text{B}-\text{N}$  vibration modes was found at  $1,576\text{ cm}^{-1}$  (**19**) and  $1,493\text{ cm}^{-1}$  (**20**), respectively [91].



#### 4.4 SEM Analysis

SEM images of the as-synthesized POMA/HCl are shown in **Figure 16**.

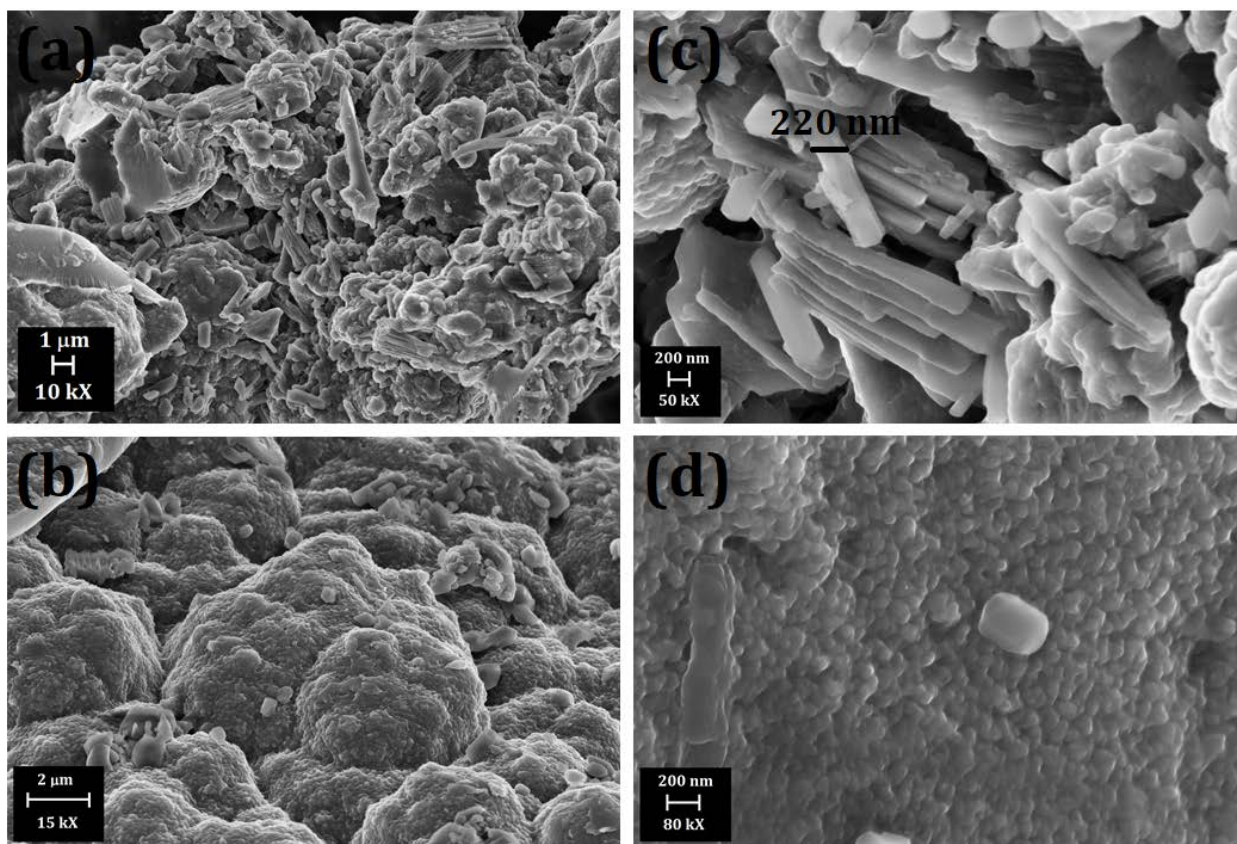


**Figure 16** - SEM images of the as-synthesized POMA/HCl.

Two different morphologies were observed: cauliflower and nanorods. **Figure 16(a)** (1  $\mu\text{m}$ ; 10 kX) shows the coexistence of these two morphologies. **Figure 16(b)** (2  $\mu\text{m}$ ; 15 kX) highlights the cauliflower morphology resulting in a considerably rough surface. **Figure 16(d)** (200 nm, 80 kX) highlights the cauliflower surface, showing that it is constituted of granules smaller than 200 nm. **Figure 16(c)** (200 nm, 50 kX) highlights the nanorods morphology, which presented an approximate diameter of 180 – 230 nm and average length about 1.6  $\mu\text{m}$ . The HCl concentration (2 M) used in the polymerization of *o*-methoxyaniline was crucial to result in multimorphologies such as cauliflower and nanorods, since previous work[5] reported a vesicular morphology (hollow spheres) of POMA when 1M HCl was used in the chemical oxidative polymerization.

SEM images of the as-synthesized POMA/HNO<sub>3</sub> are shown in **Figure 17**. The doping performed by HNO<sub>3</sub> resulted in particles tending to the spherical shape, as shown in **Figure 17(a)** (2  $\mu\text{m}$ ; 5 kX). Some images, such as **Figure 17(d)** (2  $\mu\text{m}$ ; 15 kX) and **Figure 17(f)** (200 nm; 50 kX) highlighted that these particles appear to be hollow spheres with diameter of about

800 nm. **Figure 17(c)** (1  $\mu\text{m}$ ; 30 kX) highlights these *quasi*-spherical particles, showing that they are constituted of rough surfaces, which are composed of granules smaller than 10 nm. **Figure 17(b)** (2  $\mu\text{m}$ ; 15 kX) and **Figure 17(d)** show that the polymer POMA/ $\text{HNO}_3$  also presented nanorods morphology, which average diameter of about 250 nm.

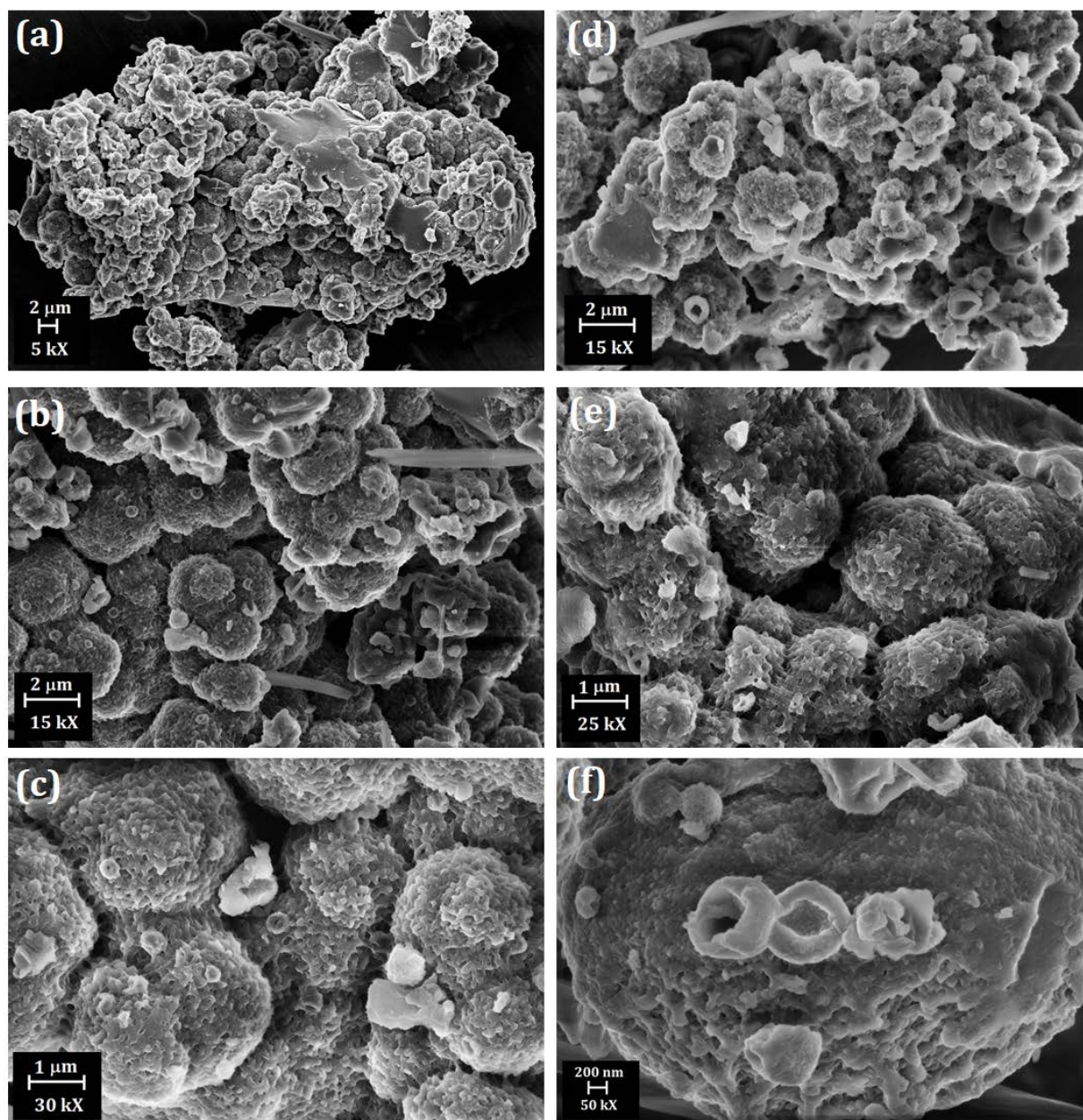


**Figure 17** - SEM images of the as-synthesized POMA/ $\text{HNO}_3$ .

SEM images of the as-synthesized POMA/ $\text{H}_2\text{SO}_4$  are shown in **Figure 18**. The doping performed by  $\text{H}_2\text{SO}_4$  resulted in particles with granular morphology, as highlighted in **Figure 18(a)** (2  $\mu\text{m}$ ; 10 kX) and **Figure 18(c)** (1  $\mu\text{m}$ ; 15 kX). Moreover, these granules presented smooth surface, as shown in **Figure 18(b)** (1  $\mu\text{m}$ ; 30 kX) and **Figure 18(d)** (200 nm; 50 kX).



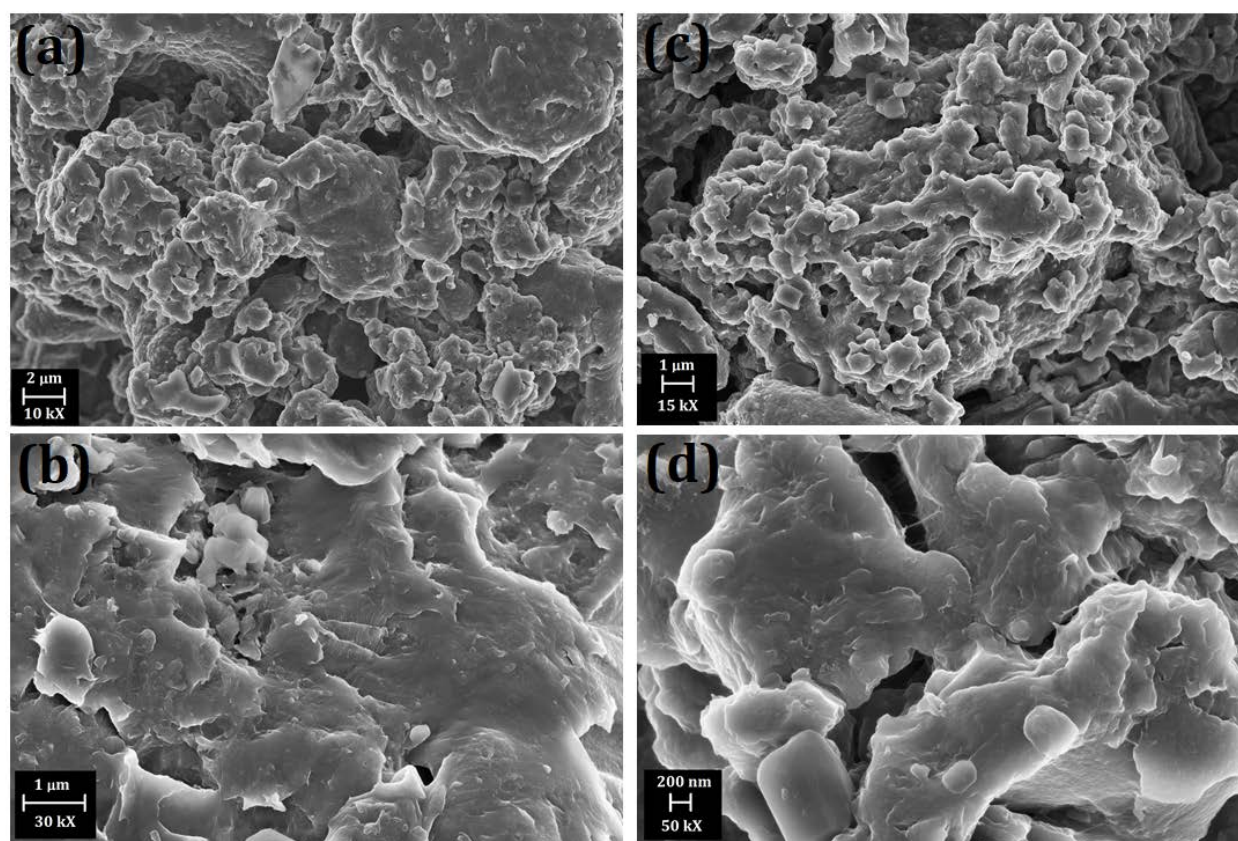


**Figure 18** - SEM images of the as-synthesized POMA/H<sub>2</sub>SO<sub>4</sub>.

SEM images of the as-synthesized POMA/H<sub>3</sub>PO<sub>4</sub> are shown in **Figure 19**. Two different morphologies were observed: granules and nanorods; however, the nanorod morphology was more evident here than in the polymers POMA/HCl and POMA/HNO<sub>3</sub>. The granular morphology was better observed in **Figure 19(b)** (1 μm; 30 kX) and **Figure 19(d)** (200 nm; 50 kX).

Each synthesized polymer presented specific morphology, which was considerably related to the nature and concentration of the dopant acids. The influence of these dopants on the morphology of conjugated polymers have been reported in scientific literature. Moreover, the nature of the ring substituent at *meta*, *ortho* or *para* positions is significantly important as well. The side groups of aniline derivatives have resulted in different morphologies. Polyaniline presented nanofiber morphology in most of the reported studies[78]. However, polymerization methodology (conventional or interfacial), as well as dopant acid concentration resulted in multimorphologies observed in a single polymer[5,78], including nanoflowers, nanotubes, nanofibers and nanoplates. The *o*-OCH<sub>3</sub> (POMA) and *o*-OCH<sub>2</sub>CH<sub>3</sub> (POEA) groups presented in the aromatic ring of aniline influence on the polymerization and morphology, resulting in hollow microspheres[5,92,93] when it were synthesized using HCl 1M.

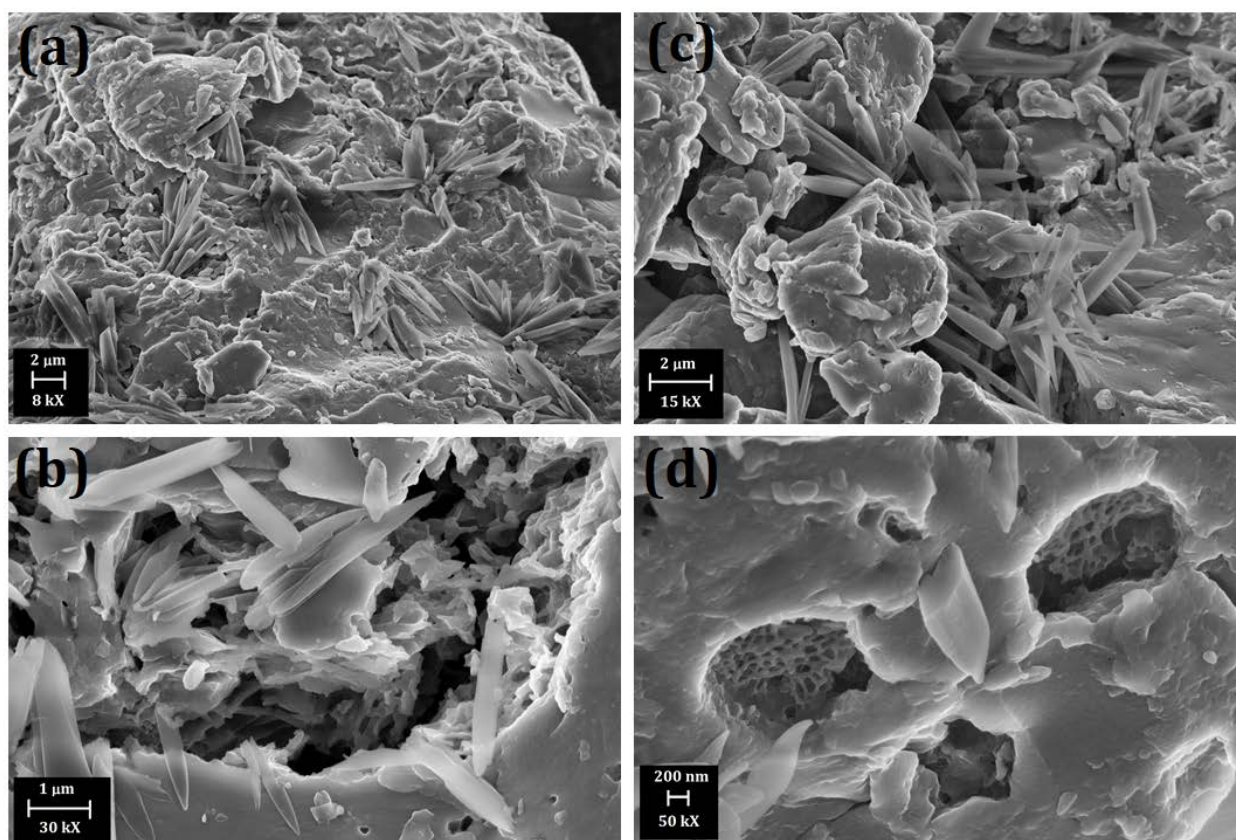


**Figure 19** - SEM images of the as-synthesized POMA/H<sub>3</sub>PO<sub>4</sub>.

Some works have reported that well crystallized polymers do not necessarily have a well- defined morphology: hollow spheres of POMA were ruptured at high time of synthesis resulting in undefined morphology with increased crystallinity and electrical conductivity[5]. In contrast, a well-defined morphology does not mean a high percentage of crystallinity either. This fact can be observed in the present work: although the polymer POMA/H<sub>3</sub>PO<sub>4</sub> presented significant amount of nanorods, it was the one with the lowest crystallinity, while granular morphology was related to better crystallinity. Our results showed that one single polymer can present multimorphologies, which may be influenced by several parameters, specially the nature and concentration of the doping acid.

#### 4.5 TG/dTG Analysis

TG/dTG curves of the polymers POMA/HCl, POMA/HNO<sub>3</sub>, POMA/H<sub>2</sub>SO<sub>4</sub> and POMA/H<sub>3</sub>PO<sub>4</sub> are shown in **Figure 20**. **Table 3** describes the main observed events and the thermal behavior of the evaluated polymers. The first thermal event was observed from 27 °C

to 125 °C for all polymers, and it was attributed to the moisture release. The mass loss released in this event was higher for the polymer POMA/HCl (around 16 %), while for POMA/HNO<sub>3</sub> and POMA/H<sub>3</sub>PO<sub>4</sub> it was found around 9 %[94,95].

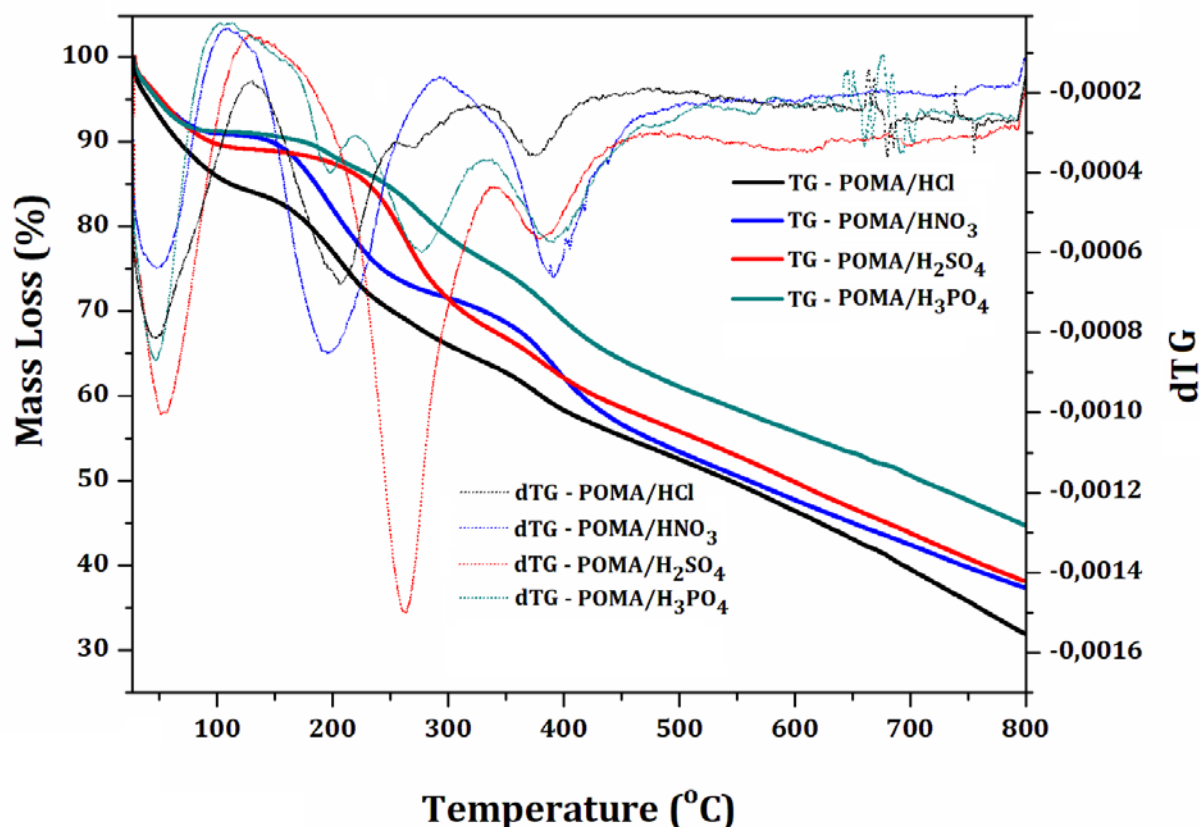


**Figure 20** - TG/dTG curves of the polymers POMA/HCl, POMA/HNO<sub>3</sub>, POMA/H<sub>2</sub>SO<sub>4</sub> and POMA/H<sub>3</sub>PO<sub>4</sub>.

**Table 3** - TGA/dTG events of the polymers POMA/HCl, POMA/HNO<sub>3</sub>, PMA/H<sub>2</sub>SO<sub>4</sub> and POMA/H<sub>3</sub>PO<sub>4</sub>.

Polymer	1° Event (°C)	Mass Loss	2° Event (°C)	Mass Loss	3° Event (°C)	Mass Loss	4° Event (°C)	Mass Loss
POMA/HCl	27-125	16%	125-255	14.5%	255-322	4.9%	332-430	8.0%
POMA/HNO <sub>3</sub>	27-125	9%	125-290	19%	---	---	290-461	16.1%
POMA/H <sub>2</sub> SO <sub>4</sub>	27-125	11.1%	150-340	21.5%	---	---	340-458	9.3%
POMA/H <sub>3</sub> PO <sub>4</sub>	27-125	9%	125-220	4%	220-332	11%	332-462	12.6%

The second event observed for the polymer POMA/H<sub>3</sub>PO<sub>4</sub> and the third event for the polymer POMA/HCl were found at around 200 °C and 280 °C, respectively. Both events were attributed to the release of coordinated water molecules. The second event for the polymers POMA/H<sub>2</sub>SO<sub>4</sub>, POMA/HNO<sub>3</sub> and POMA/HCl, and the third event for the polymer POMA/H<sub>3</sub>PO<sub>4</sub>



were observed at 255 °C, 200 °C, 220 °C, and 260 °C, respectively. These events were attributed to dopant release[76,94,96]. The polymer POMA/H<sub>2</sub>SO<sub>4</sub> presented higher mass loss of dopant release and it may be related to the release of sulfonic groups. Moreover, larger counterions such as HSO<sub>4</sub><sup>-</sup> and H<sub>2</sub>PO<sub>4</sub><sup>-</sup> seemed to require larger amount of energy to be released[97,98]. This thermal event was related to the largest percentage of mass loss (21,5 %) due to the release of sulfonic groups. Previous work also observed major mass loss regimes in the TGA curve of sulfonated polyaniline[99].

The fourth event observed in all polymers was attributed to the polymer chain degradation. Thermal stability was improved in all polymers when compared to other studies on POMA, which report degradation temperature around 300 °C[94,100]. The most thermally stable polymer, i.e., presenting polymer chain degradation started at higher temperature was POMA/H<sub>3</sub>PO<sub>4</sub> (at 398 °C), followed by POMA/HNO<sub>3</sub> (at 390 °C). The polymers POMA/H<sub>2</sub>SO<sub>4</sub> and POMA/HCl presented polymer chain degradation at 382 °C and 375 °C, respectively. The lowest mass loss of the polymer POMA/H<sub>3</sub>PO<sub>4</sub> is in agreement with previous reports[101]. The results described herein can be attributed to the nature of the dopant acids. These results suggest the thermal stability of POMA/H<sub>3</sub>PO<sub>4</sub> is higher than others.

## 4.6 Complex Impedance Spectroscopy Analysis

The structure of a polymer network is normally determined by polymer chains of different lengths that are disordered and have some random orientation. Commonly, the density of charge carriers (polaron or bipolaron) is constant in these materials[102]. The conductive process can be a result of long-range hops across each chain or over interconnected clusters. The conditions of sample preparation and doping considerably influence on the conduction mechanism. During processing, the so-called driving paths are created which can be long (favoring the conductive process) or short (making the conductive process difficult)[102–104].

On the other hand, it has been experimentally shown that the AC electrical conductivity ( $\sigma_{ac}$ ) of many materials, including polymers, has characteristic responses as a function of frequency.[102] In the low frequency region,  $\sigma_{ac}$  does not vary with the increase of frequency, so it is known as DC conductivity ( $\sigma_{dc}$ ). From a critical frequency value, a dispersion process is observed and visualized as an increment in the values of  $\sigma_{ac}$ .

**Figure 21** shows the AC electrical conductivity as a function of the frequency for the polymers POMA/HCl, POMA/HNO<sub>3</sub>, POMA/H<sub>2</sub>SO<sub>4</sub> and POMA/H<sub>3</sub>PO<sub>4</sub>. All polymers exhibited similar and typical behavior to those reported for other materials[102,103,105,106]. The electrical conductivity of POMA was found to be considerably dependent on the counterion size. For the polymer POMA/H<sub>3</sub>PO<sub>4</sub> (green curve) the  $\sigma_{dc}$  total (low frequency region) was not obtained for the considered frequency range.

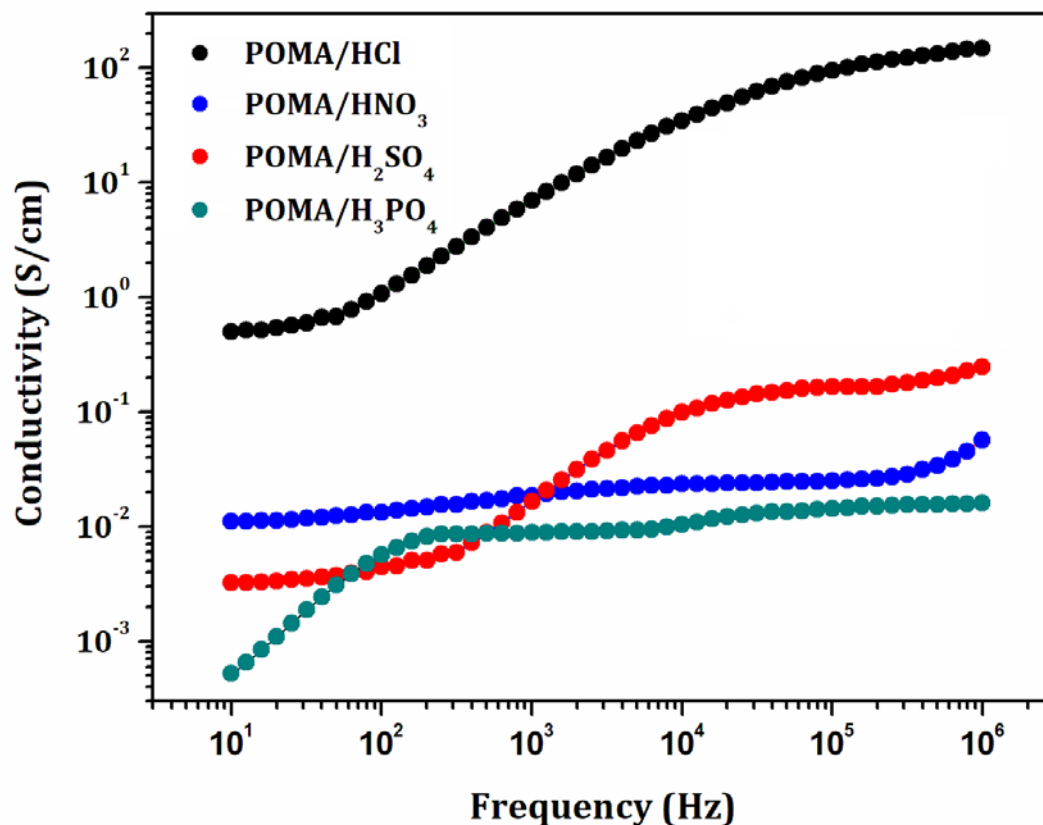


**Figure 21** - AC electrical conductivity as a function of the frequency for the polymers POMA/HCl, POMA/HNO<sub>3</sub>, POMA/H<sub>2</sub>SO<sub>4</sub> and POMA/H<sub>3</sub>PO<sub>4</sub>.

The scientific literature reported that several factors influence on the mobility of counterions along the polymer chains in polyaniline and its derivatives. These factors are related to (i) the different synthesis methodologies[107–109], (ii) the regular packing of the polymer chains (or polymer crystallinity), (iii) the ring side group at the *ortho*, *meta* or *para* positions[103,110–112], (iv) the nature of the doping acid and counterion size[113], as well as (v) possible interactions between counterions and the ring side group.

The electrical conductivity calculated for the polymer POMA/HCl was  $6.60 \times 10^{-1}$  S/cm. This value may be related to a smaller counterion size generated by hydrochloric acid used as a dopant, as well as an efficient doping process. On the other hand, this polymer presented high

percentage of crystallinity. Values of  $\sigma_{dc}$  similar to those reported in this paper were obtained by other authors using different materials and a potential of 1.5 V, triple the value employed in this paper[105,114].

Lower values of DC electrical conductivity were obtained for the polymers POMA/HNO<sub>3</sub>, POMA/H<sub>2</sub>SO<sub>4</sub> and POMA/H<sub>3</sub>PO<sub>4</sub> ( $1.11 \times 10^{-2}$  S/cm,  $3.64 \times 10^{-3}$  S/cm and  $5.21 \times 10^{-4}$  S/cm, respectively). In the case of POMA/H<sub>3</sub>PO<sub>4</sub> the conductivity value of DC was barely estimated since the constant region at low frequencies was out of measured window. These values can be justified by the increased size of the acid-related counterion, as well as by the doping process.

The less conducting polymer was obtained using H<sub>3</sub>PO<sub>4</sub> as dopant, POMA/H<sub>3</sub>PO<sub>4</sub>. This may be associated with a more random ordering compared to the other polymers, which would make it difficult for load carriers to move through the material structure. In fact, this was the less crystalline polymer as mentioned before. Furthermore, its larger counterion also would demand an increase of energy involved in the charge carrier mobility process. At low frequency a different behavior was observed: unlike the other synthesized polymers, the electrical conductivity increased by more than one order of magnitude between  $10^1$  and  $10^3$  Hz. As there are still small regions with some molecular organization, such regions can be considered as small conducting islands. Since inter- and intrachain mobility is not favored by the low percentage of crystallinity, the mobility mechanism in the polymer POMA/H<sub>3</sub>PO<sub>4</sub> may be the interparticle mobility: as the frequency increases, the charge carriers move over these conducting islands, explaining the increase of the electrical conductivity from  $10^1$  Hz.

Being an acid of high dissociation and doping power, the HCl dopant allowed the highest electrical conductivity observed in the polymer POMA/HCl. In addition, this polymer presented high crystallinity, besides the chloride contraction has the smallest size, favoring the charge mobility. At low frequency, the interparticle mobility was also observed.

The polymers POMA/HNO<sub>3</sub> and POMA/H<sub>2</sub>SO<sub>4</sub> showed similar electrical conductivity values. However, since POMA/HNO<sub>3</sub> counterions are smaller than that of POMA/H<sub>2</sub>SO<sub>4</sub>, the electrical conductivity may have been improved by the greater mobility of the charge carriers of POMA/HNO<sub>3</sub>. However, from  $10^2$  Hz the interparticle mobility mechanism was observed in POMA/H<sub>2</sub>SO<sub>4</sub>. The large size and molecular geometry of this counterion may results in low electrostatic attraction force between this contraction and the charge carriers. Once weakly attracted to the polymer chain, these counterions and the charge carriers may be easier for interparticle mobility when the frequency was increased. In contrast, this fact may also be related to the interparticle mobility of the POMA/HNO<sub>3</sub>, in which it is observed only at much



higher frequency, around  $10^5$  Hz, probably due to the greater electrostatic interaction between this small counterion and the charge carriers.

The electrical conductivity of conjugated polymers, such as polyaniline and its derivatives, has been reported over a wide range of values. This is due to the fact that the synthesis methodology has a direct influence on the structure and morphology of the resulting polymers, such as type of dopant acid, time and temperature of polymerization, concentration of reagents, etc.

The electrical conductivity of POMA was previously reported about  $8.89 \times 10^{-7}$  S/cm when prepared using 1M HCl[81]. Previous report[115] compared the electrical conductivity of polyanilines synthesized by oxidative polymerization and electropolymerization methods, and found that the chemical synthesis resulted in three-fold higher values, around  $6.3 \cdot 10^{-4}$  S/cm. Another work[95] report copolymers of PANI and POMA, measuring the conductivity of the composite and each polymer separately, reaching values of  $6 \cdot 10^{-2}$  S/cm. These results suggest that the counterion (especially its size) plays an important role in determining the conductivity, although other factors, such as the polar factor of the counterion, geometry of coordination etc., also cannot be neglected. Thus, the electrical conductivity values found for PANI and POMA are quite varied and dependent on the method of obtaining and synthesis methodology.

## CONCLUSIONS

The doped POMA polymers were successfully prepared. Their structural, morphological, thermal and electrical properties were significantly related to the nature of the dopant acid. The doping acid influenced on the polymer crystallinity, and angular displacements of diffraction peaks were associated to changes in lattice parameters. The polymers presented tetrameric molecules arranged along the [001] direction. The unit cell parameters along [100] and [010] directions were considerably influenced by the counterions; however, crystallites seemed to reach a maximum average size, independently of the percentage of crystallinity or the nature of the counterion. Each synthesized polymer presented specific morphology, which was considerably related to the nature and concentration of the dopant acids. Moreover, well-defined morphology was not related to high percentage of crystallinity. The most thermally stable polymer was POMA/HCl, followed by POMA/H<sub>3</sub>PO<sub>4</sub>. The electrical conductivity of POMA was found to be considerably dependent on the counterion size: the polymer POMA/HCl presented the highest conductivity value among all the polymers studied herein, while the polymers POMA/HNO<sub>3</sub>, POMA/H<sub>2</sub>SO<sub>4</sub> and POMA/H<sub>3</sub>PO<sub>4</sub> presented light semiconductor behavior. High electrical conductivity was observed in the polymer POMA/HCl probably due to its smaller counterion size, as well as an efficient doping process. However, the electrical conductivity of the polymer POMA/H<sub>3</sub>PO<sub>4</sub> increased by more than one order of magnitude between 10<sup>1</sup> and 10<sup>3</sup> Hz due to the interparticle mobility. Thus, we reported here a detailed systematic characterization of the emeraldine-salt form of poly(*o*-methoxyaniline) as a function of different doping acid.

## ACKNOWLEDGMENTS

This work was supported by Conselho Nacional de Desenvolvimento Científico e Tecnológico (CNPq - Grant Number 305161/2017-2), Fundação de Amparo à Pesquisa do Estado do Amazonas (FAPEAM), Coordenação de Aperfeiçoamento de Pessoal de Nível Superior (CAPES) and Laboratório de Materiais (LabMat - UFAM).

## REFERENCES

- [1] Z.T. De Oliveira, M.C. Dos Santos, Relative stability of polarons and bipolarons in emeraldine oligomers: A quantum chemical study, *Solid State Commun.* 114 (2000) 49–53. doi:10.1016/S0038-1098(99)00580-3.
- [2] D. Gonçalves, D.S. dos Santos, L.H.C. Mattoso, F.E. Karasz, L. Akcelrud, R.M. Faria, Poly (o-methoxy aniline): solubility, deprotonation-protonation process in solution and cast films, *Synth. Met.* 90 (1997) 5–11. doi:10.1016/S0379-6779(97)03895-2.
- [3] S.C. Kim, P. Huh, J. Kumar, B. Kim, J.O. Lee, F.F. Bruno, L.A. Samuelson, Synthesis of polyaniline derivatives via biocatalysis, *Green Chem.* 9 (2007) 44–48. doi:10.1039/b606839a.
- [4] V. Bavastrello, T.B. Correia Terencio, C. Nicolini, Synthesis and characterization of polyaniline derivatives and related carbon nanotubes nanocomposites - Study of optical properties and band gap calculation, *Polymer (Guildf).* 52 (2011) 46–54. doi:10.1016/j.polymer.2010.10.022.
- [5] E.A. Sanches, J.C. Soares, A.C. Mafud, G. Trovati, E.G. Fernandes, Y.P. Mascarenhas, Structural and morphological characterization of chloride salt of conducting poly(o-methoxyaniline) obtained at different time synthesis, *J. Mol. Struct.* 1039 (2013) 167–173. doi:10.1016/j.molstruc.2012.12.025.
- [6] E.A. Sanches, L.C.A. Gomes, J.C. Soares, R. Geisiane, Y.P. Mascarenhas, Characterization of Poly (o-methoxyaniline ) Emeraldine-base form obtained at different time neutralization, *J. Mol. Struct.* 1063 (2014) 336–340. doi:10.1016/j.molstruc.2014.01.082.
- [7] P. Kar, Influence of Properties of Conjugated Polymer on Doping, in: *Doping Conjug. Polym.*, John Wiley & Sons, Inc., Hoboken, NJ, USA, 2013: pp. 81–96. doi:10.1002/9781118816639.ch5.
- [8] A. Le Bail, Whole powder pattern decomposition methods and applications: A retrospection, *Powder Diffr.* 20 (2005) 316–326. doi:10.1154/1.2135315.
- [9] A.J. Heeger, Semiconducting and Metallic Polymers: The Fourth Generation of Polymeric Materials (Nobel Lecture) Copyright(c) The Nobel Foundation 2001. We thank the Nobel Foundation, Stockholm, for permission to print this lecture., *Angew. Chem. Int. Ed. Engl.* 40 (2001) 2591–2611. doi:10.1002/1521-3773(20010716)40:14<2591::AID-ANIE2591>3.0.CO.
- [10] A.G. Macdiarmid, Synthetic Metals: A Novel Role for Organic Polymers (Nobel Lecture),

Chem. Int Ed. 40 (2001). doi:1433-7851/01/4014-2581.

- [11] E.S. Medeiros, J.E. Oliveira, L.G. Paterno, L.H.C. Mattoso, Uso de Polímeros Condutores em Sensores. Parte 1: Introdução aos Polímeros Condutores, *Rev. Eletrônica Mater. e Process.* 2 (2012) 62–77.
- [12] N.K. Guimard, N. Gomez, C.E. Schmidt, Conducting polymers in biomedical engineering, *Prog. Polym. Sci.* 32 (2007) 876–921. doi:10.1016/j.progpolymsci.2007.05.012.
- [13] R. Faez, C. Reis, P.S. de Freitas, O.K. Kosima, G. Ruggeri, M.-A. de Paoli, Polímeros Condutores, *Química Nov. Na Esc.* 11 (2000) 13–18. doi:10.1017/CBO9781107415324.004.
- [14] T.F. Otero, *Conducting Polymers Bioinspired Intelligent Materials and Devices*, Royal Society of Chemistry, Cambridge, UK, 2016. doi:10.1039/9781782623748-FP001.
- [15] N.C. Greenham, R.H. Friend, *Semiconductor Device Physics of Conjugated Polymers*, *Solid State Phys. - Adv. Res. Appl.* 49 (1996) 1–149. doi:10.1016/S0081-1947(08)60297-0.
- [16] H.S. NALWA, *Organic conductive molecules and polymers*, John Wiley, 1997.
- [17] M. Pope, H.E. Swenberg, *Electronic processes in organic crystals and polymers*, Oxford Press, 1999.
- [18] F. Lux, Properties of electronically conductive polyaniline: a comparison between well-known literature data and some recent experimental findings, *Polymer (Guildf)*. 35 (1994) 2915–2936. doi:10.1016/0032-3861(94)90402-2.
- [19] W.D. Callister, JR, D.G. Rethwisch, *Materials Science and Engineering : An Introduction*, John Wiley & Sons, Inc., 2014.
- [20] I. a. Hümmelgen, L.S. Roman, J.R. De Lima, Polímeros conjugados como camada ativa de diodos emissores de luz e fotodetectores, *Polímeros*. 8 (1998) 55–63. doi:10.1590/S0104-14281998000300008.
- [21] I.F.L. Dias, M.A.T. Silva, *Polímero Semicondutores*, Livraria da Física, 2012.
- [22] A. Banerji, M.W. Tausch, U. Scherf, Classroom Experiments and Teaching Materials on OLEDs with Semiconducting Polymers, *Educ. Química*. 24 (2013) 17–22. doi:10.1016/s0187-893x(13)73190-2.
- [23] P. Kar, *Doping in Conjugated Polymers*, Wiley, n.d.
- [24] Y. Andreu, S. De Marcos, J.R. Castillo, J. Galbán, Sensor film for Vitamin C determination based on absorption properties of polyaniline, *Talanta*. 65 (2005) 1045–1051. doi:10.1016/j.talanta.2004.08.036.
- [25] R.B. Kaner, A.G. MacDiarmid, *Plastics That Conduct Electricity.*, *Sci. Am.* 258 (1988) 106–

111. doi:10.1038/scientificamerican0288-106.

- [26] F.S. Borges, *Elementos de cristalografia*, 2nd ed., Fundação Lacoste Gulbenkian., Lisboa, 1980.
- [27] V.N. Prigodin, A.J. Pstein, *Charge Transport in Conducting Polymers*, in: *Introd. to Org. Electron. Optoelectron. Mater. Devices*, CRC Press, 2017: pp. 101–141.
- [28] A. J. Heeger, *Polyaniline with surfactant counterions: Conducting polymer materials which are processible in the conducting form*, *Synth. Met.* 57 (1993) 3471–3482. doi:10.1016/0379-6779(93)90462-6.
- [29] Y. Xia, J.M. Wiesinger, A.G. MacDiarmid, A.J. Epstein, *Camphorsulfonic Acid Fully Doped Polyaniline Emeraldine Salt: Conformations in Different Solvents Studied by an Ultraviolet/Visible/ Near-Infrared Spectroscopic Method*, *Chem. Mater.* 7 (1995) 443–445. doi:10.1021/cm00051a002.
- [30] W.J. Feast, J. Tsibouklis, K.L. Pouwer, L. Groenendaal, E.W. Meijer, *Synthesis, processing and material properties of conjugated polymers*, *Polymer (Guildf)*. 37 (1996) 5017–5047. doi:10.1016/0032-3861(96)00439-9.
- [31] V.G. Kulkarni, L.D. Campbell, W.R. Mathew, *Thermal stability of polyaniline*, *Synth. Met.* 30 (1989) 321–325.
- [32] A.J. Epstein, *Conducting Polymers: Electrical Conductivity*, in: *Phys. Prop. Polym. Handb.*, 2nd ed., Springer, 2007.
- [33] J. Tarver, Y.-L. Loo, CHAPTER 12. *Polyanilines*, in: *Conjug. Polym. A Pract. Guid. to Synth.*, 2013: pp. 248–264. doi:10.1039/9781849739771-00248.
- [34] A.J. Epstein, J.M. Ginder, F. Zuo, R.W. Bigelow, W.-S.H. and A.G.M.D. H.-S. Woo and D.B. Tanner; and A.F. Richter, *Insulator To Metal Transition In Polyaniline*, 18 (1987) 303–309.
- [35] G.M. do Nascimento, *Resonance Raman of polyanilines nanofibers*, in: *Adv. Conduct. Polym. Res.*, 2015.
- [36] L.H.C. Mattoso, *Polyanilines: Synthesis, structure and properties*, *Quim. Nova.* 19 (1996) 388–399.
- [37] Y. XIA, *Polyanilines: synthesis, conformational structures and applications*, in: *Electr. Opt. Polym. Syst.*, Marcel Dekker, New York, NY, 1998: pp. 359 – 386.
- [38] J.H. Sung, S.J. Kim, K.H. Lee, *Preparation of compact polyaniline films: Electrochemical synthesis using agar gel template and charge-storage applications*, *J. Power Sources.* 126 (2004) 258–267. doi:10.1016/j.jpowsour.2003.08.015.

- [39] B. Angaleeswari, R.M. Dura Amirtham, T. Jeevithaa, V. Vaishnavi, T. Eevera, S. Berchmans, V. Yegnaraman, Poly(*o*-anisidine)-anion composite films as sensing platform for biological molecules, *Sensors Actuators, B Chem.* 129 (2008) 558–565. doi:10.1016/j.snb.2007.09.003.
- [40] W.A. Gazotti Junior, Preparação e caracterização da poli(*o*-metoxianilina) dopada como ácidos funcionalizados e sua utilização em aplicações de interesse tecnológico, (1998) 166.
- [41] S.P. Armes, J.F. Miller, Optimum reaction conditions for the polymerization of aniline in aqueous solution by ammonium persulphate, *Synth. Met.* 22 (1988) 385–393. doi:10.1016/0379-6779(88)90109-9.
- [42] G.M. Morales, M. Llusà, M.C. Miras, C. Barbero, Effects of high hydrochloric acid concentration on aniline chemical polymerization, *Polymer (Guildf).* 38 (1997) 5247–5250. doi:10.1016/S0032-3861(97)82751-6.
- [43] C. Eiras, I.N.G. Passos, A.C.F. De Brito, J.R. Dos Santos, V. Zucolotto, O.N. Oliveira, I.L. Kitagawa, C.J.L. Constantino, H.N. Da Cunha, Nanocompósitos eletroativos de poli-*o*-metoxianilina e polissacarídeos naturais, *Quim. Nova.* 30 (2007) 1158–1162. doi:10.1590/S0100-40422007000500020.
- [44] D.W. Hatchett, M. Josowicz, J. Janata, Acid doping of poly aniline: Spectroscopic and electrochemical studies, *J. Phys. Chem. B.* 103 (1999) 10992–10998. doi:10.1021/jp991110z.
- [45] J.P. Pouget, M.E. Józefowicz, A.J. Epstein, X. Tang, A.G. MacDiarmid, X-ray structure of polyaniline, *Macromolecules.* 24 (1991) 779–789. doi:10.1021/ma00003a022.
- [46] K. Tashiro, M. Kobayashi, T. Kawai, K. Yoshino, Crystal structural change in poly(3-alkyl thiophene)s induced by iodine doping as studied by an organized combination of X-ray diffraction, infrared/Raman spectroscopy and computer simulation techniques, *Polymer (Guildf).* 38 (1997) 2867–2879. doi:10.1016/S0032-3861(96)00876-2.
- [47] P.P. Sengupta, P. Kar, B. Adhikari, Influence of dopant in the synthesis, characteristics and ammonia sensing behavior of processable polyaniline, *Thin Solid Films.* 517 (2009) 3770–3775. doi:10.1016/j.tsf.2008.12.049.
- [48] N. Aydemir, J. Malmstro, J. Travas-sejdic, Conducting polymer based electrochemical biosensors, (2016) 8264–8277. doi:10.1039/c5cp06830d.
- [49] J. Janata, M. Josowicz, Conducting polymers in electronic chemical sensors, *Nat. Mater.* 2 (2003) 19–24. doi:10.1038/nmat768.

- [50] F. Kong, Y. Wang, J. Zhang, H. Xia, B. Zhu, Y. Wang, S. Wang, S. Wu, The preparation and gas sensitivity study of polythiophene/SnO<sub>2</sub> composites, *Mater. Sci. Eng. B Solid-State Mater. Adv. Technol.* 150 (2008) 6–11. doi:10.1016/j.mseb.2008.01.003.
- [51] H.K. Jun, Y.S. Hoh, B.S. Lee, S.T. Lee, J.O. Lim, D.D. Lee, J.S. Huh, Electrical properties of polypyrrole gas sensors fabricated under various pretreatment conditions, *Sensors Actuators, B Chem.* 96 (2003) 576–581. doi:10.1016/j.snb.2003.06.002.
- [52] S. Virji, J. Huang, R.B. Kaner, B.H. Weiller, Polyaniline nanofiber gas sensors: Examination of response mechanisms, *Nano Lett.* 4 (2004) 491–496. doi:10.1021/nl035122e.
- [53] M.E. Nicho, M. Trejo, A. García-Valenzuela, J.M. Saniger, J. Palacios, H. Hu, Polyaniline composite coatings interrogated by a nulling optical-transmittance bridge for sensing low concentrations of ammonia gas, *Sensors Actuators, B Chem.* 76 (2001) 18–24. doi:10.1016/S0925-4005(01)00562-7.
- [54] J. Arias-Pardilla, T.F. Otero, J.G. Martínez, Y.A. Ismail, Biomimetic Sensing – Actuators Based on Conducting Polymers, *Asp. Fundam. Appl. Conduct. Polym.* (2012). doi:10.5772/29348.
- [55] G. Alici, G. Spinks, N.N. Huynh, L. Sarmadi, R. Minato, Establishment of a biomimetic device based on tri-layer polymer actuators - Propulsion fins, *Bioinspiration and Biomimetics.* 2 (2007) 17–30. doi:10.1088/1748-3182/2/2/S03.
- [56] T. Shoa, J.D. Madden, N. Fekri, N.R. Munce, V.X.D. Yang, Conducting polymer based active catheter for minimally invasive interventions inside arteries, *Proc. 30th Annu. Int. Conf. IEEE Eng. Med. Biol. Soc. EMBS'08 - "Personalized Healthc. through Technol.* (2008) 2063–2066. doi:10.1109/iembs.2008.4649598.
- [57] Y. Naka, M. Fuchiwaki, K. Tanaka, Amicropump driven by a polypyrrole-based conducting polymer soft actuator, *Polym. Int.* 59 (2010) 352–356. doi:10.1002/pi.2762.
- [58] X. He, C. Li, F. Chen, G. Shi, Polypyrrole microtubule actuators for seizing and transferring microparticles, *Adv. Funct. Mater.* 17 (2007) 2911–2917. doi:10.1002/adfm.200600869.
- [59] A.U. Agobi, H. Louis, T.O. Magu, P.M. Dass, A Review on Conducting Polymers-Based Composites for Energy Storage Application, *J. Chem. Rev.* 1 (2019) 19–34. doi:10.33945/sami/jcr.2019.1.1934.
- [60] Y. Shi, L. Peng, Y. Ding, Y. Zhao, G. Yu, Nanostructured conductive polymers for advanced energy storage, *Chem. Soc. Rev.* 44 (2015) 6684–6696. doi:10.1039/c5cs00362h.
- [61] T. Houghton, G. Eltohamy, H. Yu, I.A. Fulton, An Experimental Magnesium Ion Battery Cell Made of Flexible Materials, (2017). doi:10.1109/ECTC.2017.330.

- [62] N. Yi, M.R. Abidian, Conducting polymers and their biomedical applications, *Biosynthetic Polym. Med. Appl.* (2015) 243–276. doi:10.1016/B978-1-78242-105-4.00010-9.
- [63] Manju.Gerard, Ashab.Choubey, B.D.Malhotra, Review: Application of Conducting Polymer to Biosensors, *Biosens. Bioelectron.* 17 (2001) 345–359.
- [64] G. Mei, D. Liming, G.W. Gordon, Biosensors Based on Aligned Carbon Nanotubes Coated with Inherently Conducting Polymers, *Electroanalysis.* 15 (2003) 1089–1094.
- [65] P.B. Lippa, L.J. Sokoll, D.W. Chan, Immunosensors - Principles and applications to clinical chemistry, *Clin. Chim. Acta.* 314 (2001) 1–26. doi:10.1016/S0009-8981(01)00629-5.
- [66] E.A. Sanches, J.C. Soares, R.M. Iost, V.S. Marangoni, G. Trovati, T. Batista, A.C. Mafud, V. Zucolotto, Y.P. Mascarenhas, Structural characterization of emeraldine-salt polyaniline/gold nanoparticles complexes, *J. Nanomater.* 2011 (2011) 1–7. doi:10.1155/2011/697071.
- [67] D.K. Sambhu Bhadra, Nikhil K. Singha, Electrochemical Synthesis of Polyaniline and Its Comparison with Chemically Synthesized Polyaniline, *J. Appl. Polym. Sci.* 104 (2007).
- [68] J. Rodríguez-Carvajal, An introduction to the program (Version July 2001), Lab. Leon Brillouin. (2002) 1–139.
- [69] G.S. Pawley, Unit-cell refinement from powder diffraction scans, *J. Appl. Crystallogr.* 14 (1981) 357–361. doi:10.1107/S0021889881009618.
- [70] P. Thompson, D. Cox, J. Hastings, Rietveld refinement of Debye-Scherrer synchrotron X-ray data from Al<sub>2</sub>O<sub>3</sub>, October. (1987) 79–83. doi:10.1107/s0021889887087090.
- [71] M. Evain, S. Quillard, B. Corraze, W. Wang, A.G. MacDiarmid, A phenyl-end-capped tetramer of aniline, *Acta Crystallogr. Sect. E Struct. Reports Online.* 58 (2002) o343–o344. doi:10.1107/S1600536802002532.
- [72] N.C. Popa, The (hkl) dependence of diffraction-line broadening caused by strain and size for all Laue groups in Rietveld refinement, *J. Appl. Crystallogr.* 31 (1998) 176–180. doi:10.1107/S0021889897009795.
- [73] J.A. House, K.A. House, *Descriptive Inorganic Chemistry*, Elsevier Inc., 2016.
- [74] W. Bleam, *Soil and Environmental Chemistry*, Elsevier Inc., 2017.
- [75] R.. Murugesan, E. Subramanian, Effect of organic dopants on electrodeposition and characteristics of polyaniline under the varying influence of H<sub>2</sub>SO<sub>4</sub> and HClO<sub>4</sub> electrolyte media, *Mater. Chem. Phys.* 80 (2003) 731–739.
- [76] A.A. Ferreira, E.A. Sanches, Multimorphologies of hydrochloride polyaniline synthesized by conventional and interfacial polymerization, *J. Mol. Struct.* 1143 (2017) 294–305.



doi:10.1016/j.molstruc.2017.04.104.

- [77] J.C. Soares, C. Eiras, E.A. Sanches, Electrosynthesis and optical characterization of poly(*p*-phenylene), polypyrrole and poly(*p*-phenylene)-polypyrrole Films, 17 (2014) 332–337.
- [78] E.A. Sanches, J.C. Soares, A.C. Mafud, E.G.R. Fernandes, F.L. Leite, Y.P. Mascarenhas, Structural characterization of chloride salt of conducting polyaniline obtained by XRD, SAXD, SAXS and SEM, J. Mol. Struct. 1036 (2013) 121–126. doi:10.1016/j.molstruc.2012.09.084.
- [79] J.S.M. da Silva, S.M. de Souza, G. Trovati, E.A. Sanches, Chloride salt of conducting polyaniline synthesized in the presence of CeO<sub>2</sub>: Structural analysis of the core-shell nanocomposite, J. Mol. Struct. 1127 (2017) 337–344. doi:10.1016/j.molstruc.2016.07.114.
- [80] E.A. Sanches, S.F. Alves, J.C. Soares, A.M. Da Silva, C.G. Da Silva, S.M. De Souza, H.O. Da Frota, Nanostructured polypyrrole powder: A structural and morphological characterization, J. Nanomater. 2015 (2015). doi:10.1155/2015/129678.
- [81] E.A. Sanches, L.C.A. Gomes, J.C. Soares, G.R. Da Silva, Y.P. Mascarenhas, Characterization of Poly(*o*-methoxyaniline) Emeraldine-base form obtained at different time neutralization, J. Mol. Struct. 1063 (2014) 336–340. doi:10.1016/j.molstruc.2014.01.082.
- [82] E.A. Sanches, A.S. Carolino, A.L. Santos, E.G.R. Fernandes, D.M. Trichês, Y.P. Mascarenhas, The use of Le Bail Method to analyze the semicrystalline pattern of a nanocomposite based on polyaniline emeraldine-salt form and  $\alpha$ -Al<sub>2</sub>O<sub>3</sub>, Adv. Mater. Sci. Eng. 2015 (2015) 1–8.
- [83] D.J.K. Robert M. Silverstein, Francis X. Webster, Spectrometric identification of organic compounds, J. Mol. Struct. (2005) 512. doi:10.1016/0022-2860(76)87024-X.
- [84] A. Nyczyk, M. Hasik, W. Turek, A. Sniechota, Nanocomposites of polyaniline, its derivatives and platinum prepared using aqueous Pt sol, Synth. Met. 159 (2009) 561–567. doi:10.1016/j.synthmet.2008.11.019.
- [85] M. Hasik, E. Wenda, C. Paluszkiwicz, A. Bernasik, J. Camra, Poly(*o*-methoxyaniline)-palladium systems: Effect of preparation conditions on physico-chemical properties, Synth. Met. 143 (2004) 341–350. doi:10.1016/j.synthmet.2003.12.020.
- [86] J. Jiang, L.H. Ai, A.H. Liu, A novel poly(*o*-anisidine)/CoFe<sub>2</sub>O<sub>4</sub> multifunctional nanocomposite: Preparation, characterization and properties, Synth. Met. 160 (2010) 333–336. doi:10.1016/j.synthmet.2009.10.032.
- [87] M. Trchová, E.N. Konyushenko, J. Stejskal, J. Kovářová, G. Ćirić-Marjanović, The

conversion of polyaniline nanotubes to nitrogen-containing carbon nanotubes and their comparison with multi-walled carbon nanotubes, *Polym. Degrad. Stab.* 94 (2009) 929–938. doi:10.1016/j.polymdegradstab.2009.03.001.

- [88] A. Mostafaei, A. Zolriasatein, Synthesis and characterization of conducting polyaniline nanocomposites containing ZnO nanorods, *Prog. Nat. Sci. Mater. Int.* 22 (2012) 273–280. doi:10.1016/j.pnsc.2012.07.002.
- [89] D. Sangamithirai, S. Munusamy, V. Narayanan, A. Stephen, Fabrication of neurotransmitter dopamine electrochemical sensor based on poly(o-anisidine)/CNTs nanocomposite, *Surfaces and Interfaces.* 4 (2016) 27–34. doi:10.1016/j.surfin.2016.09.003.
- [90] I. Šeděnková, E.N. Konyushenko, J. Stejskal, M. Trchová, J. Prokeš, Solid-state oxidation of aniline hydrochloride with various oxidants Ivana, *Synth. Met.* 161 (2011) 1353–1360. doi:10.1016/j.synthmet.2011.04.037.
- [91] E.T. Kang, K.G. Neoh, K.L. Tan, Polyaniline: A polymer with many interesting intrinsic redox states, *Prog. Polym. Sci.* 23 (1998) 277–324. doi:10.1016/S0079-6700(97)00030-0.
- [92] A. Al-Dulaimi, S. Hashim, F.L. Abdulrazak, M. Husham, Electrical conductive polyaniline in various nanostructures for corrosion inhibition of carbon steel, *J. Mech. Eng. Sci.* 12 (2018) 3738–3749.
- [93] M. Moussa, M.F. El-kady, Z. Zhao, Recent progress and performance evaluation for polyaniline / graphene nanocomposites as supercapacitor electrodes, *Nanotechnology.* 27 (2016) 42001–42021. doi:10.1088/0957-4484/27/44/442001.
- [94] D.H.F. Kanda, J.A. Malmonge, W.F. Alves, E.C. Venancio, L.F. Malmonge, F.L. Leite, L.H.C. Mattoso, Thermo-analyses of polyaniline and its derivatives, *Thermochim. Acta.* 502 (2010) 43–46. doi:10.1016/j.tca.2010.02.003.
- [95] P. Mokreva, D. Tsocheva, G. Ivanova, L. Terlemezyan, Copolymers of aniline and o-methoxyaniline: Synthesis and characterization, *J. Appl. Polym. Sci.* 99 (2006) 75–81. doi:10.1002/app.22221.
- [96] J. Yue, Z.H. Wang, K.R. Cromack, A.J. Epstein, A.G. Macdiarmid, J. Yue, Z.H. Wang, K.R. Cromack, A.J. Epstein, A.G. Macdiarmid, Effect of sulfonic acid group on polyaniline backbone., *J. Am. Chem. Soc.* 113 (2002) 2665–2671. doi:10.1021/ja00007a046.
- [97] P. Saini, V. Choudhary, S.K. Dhawan, Electrical properties and EMI shielding behavior of highly thermally stable polyaniline/colloidal graphite composites, *Polym. Adv. Technol.*

- 20 (2009) 355–361. doi:10.1002/pat.1230.
- [98] C.H. Chen, C.J. Ko, C.H. Chuang, C.F. Mao, W.T. Liao, C.D. Hsieh, Synthesis and characterization of polyaniline co-doped with nitric acid and dodecyl benzene sulfonic acid, *J. Polym. Res.* 24 (2016). doi:10.1007/s10965-016-1175-2.
- [99] T.C. Tsai, D.A. Tree, M.S. High, Degradation Kinetics of Polyaniline Base and Sulfonated Polyaniline, *Ind. Eng. Chem. Res.* 33 (1994) 2600–2606. doi:10.1021/ie00035a011.
- [100] Inamuddin, Y.A. Ismail, Synthesis and characterization of electrically conducting poly-*o*-methoxyaniline Zr(IV) molybdate Cd(II) selective composite cation-exchanger, *Desalination.* 250 (2010) 523–529. doi:10.1016/j.desal.2008.06.033.
- [101] W. Li, M. Wan, Stability of polyaniline synthesized by a doping-dedoping-redoping method, *J. Appl. Polym. Sci.* 71 (1999) 615–621. doi:10.1002/(SICI)1097-4628(19990124)71:4<615::AID-APP13>3.0.CO;2-O.
- [102] A.N. Papathanassiou, I. Sakellis, J. Grammatikakis, Universal frequency-dependent ac conductivity of conducting polymer networks, *Appl. Phys. Lett.* 91 (2007) 0–3. doi:10.1063/1.2779255.
- [103] S. Bhadra, N.K. Singha, D. Khastgir, Effect of aromatic substitution in aniline on the properties of polyaniline, *Eur. Polym. J.* 44 (2008) 1763–1770.
- [104] J. Jin, Y. Lin, M. Song, C. Gui, S. Leesirisan, Enhancing the electrical conductivity of polymer composites, *Eur. Polym. J.* 49 (2013) 1066–1072. doi:10.1016/j.eurpolymj.2013.01.014.
- [105] I. Sakellis, A.N. Papathanassiou, J. Grammatikakis, Transformation of polarons to bipolarons in disordered matter, *Appl. Phys. Lett.* 92 (2008) 2006–2009. doi:10.1063/1.2938995.
- [106] M.A. Gabal, M.A. Hussein, A.A. Hermas, Synthesis, characterization and electrical conductivity of polyaniline-Mn<sub>0.8</sub>Zn<sub>0.2</sub>Fe<sub>2</sub>O<sub>4</sub> nano-composites, *Int. J. Electrochem. Sci.* 11 (2016) 4526–4538. doi:10.20964/2016.06.20.
- [107] M.A.C. Mazzeu, L.K. Faria, A. de M. Cardoso, A.M. Gama, M.R. Baldan, E.S. Gonçalves, Structural and morphological characteristics of polyaniline synthesized in pilot scale, *J. Aerosp. Technol. Manag.* 9 (2017) 39–47. doi:10.5028/jatm.v9i1.726.
- [108] J. Stejskal, P. Bober, M. Trchová, D. Nuzhnyy, V. Bovtun, M. Savinov, J. Petzelt, J. Proke, Interfaced conducting polymers, *Synth. Met.* 224 (2017) 109–115. doi:10.1016/j.synthmet.2016.12.029.
- [109] M. Behbahani, Y. Bide, M. Salarian, M. Niknezhad, S. Bagheri, The use of tetragonal star-like polyaniline nanostructures for efficient solid phase extraction and trace detection of

Pb (II) and Cu (II) in agricultural products , sea foods , and water samples, Food Chem. 158 (2014) 14–19. doi:10.1016/j.foodchem.2014.02.110.

- [110] A.S. Silva, J.C. Soares, A. Carolina, S.M. De Souza, E.G.R. Fernandes, Y.P. Mascarenhas, E.A. Sanches, Structural and morphological characterization of Poly(*o*-ethoxyaniline) Emeraldine-salt form using FTIR , XRD , LeBail Method and SEM, J. Mol. Struct. (2014). doi:10.1016/j.molstruc.2014.04.039.
- [111] G. Trovati, E.A. Sanches, S.M. De Souza, A.L. Dos Santos, S.C. Neto, Y.P. Mascarenhas, G.O. Chierice, Rigid and semi rigid polyurethane resins: A structural investigation using DMA, SAXS and Le Bail method, J. Mol. Struct. 1075 (2014) 589–593. doi:10.1016/j.molstruc.2014.07.024.
- [112] S.M. Sayyah, M.M. El-Rabiey, H. El-Feky, A.F. Gaber, Electropolymerization of 2-methoxyaniline: Kinetic studies, mechanism, characterization of the polymer and applications as corrosion protection for mild steel in acid medium, Int. J. Polym. Mater. Polym. Biomater. 56 (2007) 605–628. doi:10.1080/00914030600992285.
- [113] E.P. Koval'chuck, V.N. Stratan, V.O. Reshentnyak, B. J., W.S. M., Synthesis and Properties of the Polyanisidines, Solid State Ionics. (2001) 217–224. doi:10.1021/ar300348n.(2).
- [114] M. Faisal, S. Khasim, Electrical conductivity, dielectric behavior and emi shielding effectiveness of polyaniline-yttrium oxide composites, Bull. Korean Chem. Soc. 34 (2013) 99–106. doi:10.5012/bkcs.2013.34.1.99.
- [115] S. Bhadra, D. Khastgir, Determination of crystal structure of polyaniline and substituted polyanilines through powder X-ray diffraction analysis, Polym. Test. 27 (2008) 851–857. doi:10.1016/j.polymertesting.2008.07.002.